

A STUDY OF THE ATOMIC NUMBER DEPENDENCE OF CHARMED D MESON
HADROPRODUCTION

BY

ERIC MATTHEW AITALA

B.S., The Pennsylvania State University, 1988

A Thesis
Submitted to the Faculty of
The University of Mississippi
in Partial Fulfillment of the Requirements
for the Degree of Master of Science
in the Department of Physics

The University of Mississippi

August, 1993

A STUDY OF THE ATOMIC NUMBER DEPENDENCE OF CHARMED D MESON
HADROPRODUCTION

BY

ERIC MATTHEW AITALA

Assistant Professor of Physics and Astronomy
(Director of the Thesis)

F.A.P. Barnard Distinguished Professor of Physics
and Astronomy
(Chairman of the Department)

Professor of Physics and Astronomy

Assistant Professor of Physics and Astronomy

Dean of the Graduate School

ABSTRACT

A STUDY OF THE ATOMIC NUMBER DEPENDENCE OF CHARMED D MESON HADROPRODUCTION

AITALA, ERIC MATTHEW. B.S., The Pennsylvania State University, 1988. M.S., The University of Mississippi, 1993. Thesis directed by Dr. Donald J. Summers.

We have investigated the nuclear A dependence for the production of D^0 and D^+ charmed mesons in 500 GeV/c πN interactions. The data were taken by the E791 collaboration at Fermilab's Tagged Photon spectrometer and partially analyzed on a large UNIX/RISC based computer farm located at the University of Mississippi. The measurement of the A dependence for charmed meson production reveals information about the quark distribution within nucleons, specifically the quark distribution function and the nuclear cross sections. The study also reveals information on the state of the E791 reconstruction and Monte Carlo simulation.

Acknowledgments

I would like to thank Drs. Don Summers, Lucien Cremaldi, and Krish Gounder for their guidance and assistance in the preparation and writing of this thesis. Without their patience and understanding, it would have been impossible to finish this work. I would also like to thank Ali Rafatian for listening to my ramblings. Finally, I would like to thank Colin Gay and Robert Jedicke who paved the way for this line of research in E769.

TABLE OF CONTENTS

LIST OF TABLES	vii
LIST OF FIGURES	viii

Chapter	Page
I. INTRODUCTION.....	1
II. CROSS SECTION AND A-DEPENDENCE THEORY.....	3
III. THE FERMILAB TEVATRON AND THE E791 SPECTROMETER.....	9
The Fermilab Tevatron.....	9
Beam.....	10
The Tagged Photon Lab Spectrometer.....	11
Beamline PWC & SMD.....	11
Experimental Target.....	13
Trigger.....	14
Downstream SMD.....	14
Downstream PWC.....	16
Drift Chambers.....	16
Magnets.....	18
Cerenkov Counters	19
SLIC and Hadrometer.....	22
Muon Walls.....	23
IV. DATA ACQUISITION SYSTEM	24
V. DATA RECONSTRUCTION	27

Chapter	Page
VI. STRIPPING THE D MESON SIGNAL FROM THE DST TAPES.....	30
VII. THE MONTE CARLO SIMULATION.....	37
VIII. RESULTS AND DISCUSSION.....	48
IX. CONCLUSIONS.....	54
SELECTED BIBLIOGRAPHY.....	55
APPENDIX A. A SAMPLE STRIPPING SUBROUTINE.....	58
BIOGRAPHICAL SKETCH OF THE AUTHOR.....	79

LIST OF TABLES

Table		Page
1.	D Meson Statistics	1
2.	Target Information	13
3.	Drift Chamber Specifications	17
4.	Cerenkov Chamber Particle Momentum Thresholds	19
5.	Data Acquisition System	25
6.	Cuts Used in D Meson Stripping	32
7.	D ⁰ and D ⁺ Fitted Mass Plots for Each Target.	34
8.	D Meson Signals for each Target as Generated by the MC.	39
9.	Total Efficiency by Target.....	40
10.	Target Positions	42
11.	A-Dependence Values Calculated for Each Platinum-Carbon Target Pair.....	48
12.	A-Dependence Average Values	48
13.	Comparison of α Measurements	50

LIST OF FIGURES

Figure	Page
1. Charm Production by an Incident Meson on a Baryon Target.....	3
2. Layout of Accelerator and Beamline System.....	10
3. The TPL/E791 Spectrometer.....	12
4. SMD Schematic.....	15
5. Drift Chamber Wire Plane Orientation	18
6. Photomultiplier Tube Schematic	21
7. The Data Acquisition System.....	26
8. DP3 Cut Representation	33
9. D ⁰ Mass Plots	35
10. D ⁺ Mass Plots	36
11. Percent Efficiency versus Target	41
12. Primary Vertex Position.....	43
13. X-Y Primary Vertex Positions.....	43
14. IEPRM2 Histograms	46
15. Feynman X and PTB Histograms.....	47

Chapter One: Introduction

The E791 Experiment at Fermilab's Tagged Photon Lab (TPL) yielded a vast quantity of high energy physics data. The experiment collected the world's largest sample of charm quark decays. This created the necessity for a means to analyze the data in a timely and efficient manner. To this end large parallel processing computer farms were assembled at The Kansas State University, Fermilab, Rio de Janeiro, and The University of Mississippi. The amount of data, intended to study rare charm decays, also provided the opportunity to perform useful research with only a small fraction analyzed. An initial study was made concerning the atomic number dependence of the production of D^0 and D^+ charmed mesons ¹.

Table 1
D Meson Statistics [1]

	D^0	D^+
Mass (GeV)	1.864	1.869
Quark Content	$c\bar{u}$	$c\bar{d}$
Lifetime (s)	4.21×10^{-13}	10.62×10^{-13}
Primary Decay Modes	K^0X	K^0X
	K^-X	K^-X

¹The charge conjugate states of particles are implicitly included throughout this thesis.

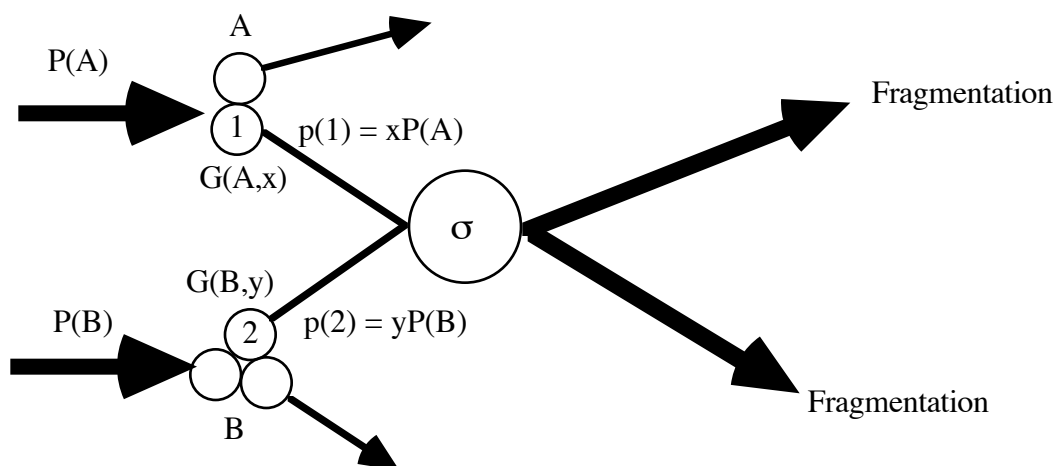
See Table 1 for D meson data. An A-dependence study should aid in determining if the cross section for charm production is proportional to the cross-sectional area, as in hard sphere scattering, or the volume of the target nuclei. This initial study will also be used to determine if any deficiencies exist in the E791 reconstruction package or the Monte Carlo simulation.

The D meson signals were gathered by searching for the decays, $D^0 \rightarrow K^- + \pi^+$ and $D^+ \rightarrow K^- + \pi^+ + \pi^+$. Once extracted, the events were examined to determine the target location of the primary interaction vertex. A Monte Carlo simulation was run to calculate and combine the detector and reconstruction efficiency, and the detector's geometrical acceptance into an overall efficiency. The data from the Monte Carlo was compared to the real data to search for inconsistencies. The raw data were corrected using this overall efficiency to get the total signal. An A-dependence was calculated based upon theory and work established in the previous experiment at TPL.

Chapter Two: Cross Section and A-Dependence Theory

The production of charm particles is a three part process. Figure 1 shows a collision between the incident meson A and the target baryon B, having a center of mass energy of \sqrt{s} . The charm quarks are produced by the sub-collision of two partons, either constituent quarks or gluons. The charm production cross-section is described by the structure functions, G , and the hard interaction cross section, σ . The momentum fraction carried by the partons is dependent upon the parent particle's distribution function and characterized by x for parton 1 and y for parton 2. The quarks formed then undergo fragmentation into real mesons and/or baryons that can be experimentally observed. The fragmentation is described by fragmentation functions that are not relevant to the determination of the charm cross section.

Figure 1
Charm Production by an Incident Meson on a Baryon Target



The total charm cross section is given by [2] :

$$\sigma_c(s) = \int_{x_{\min}}^1 dx \int_{\frac{x_{\min}}{x}}^1 dy (G(A,x)G(B,y) \sigma_{pp \rightarrow c}(s'=xys)) , \quad (2.1)$$

where:

- $G(A,x)$ and $G(B,y)$ are the structure functions for parton 1 in hadron A and parton 2 in hadron B;
- x and y are the parton momentum fractions;
- $s' = xys$ is the square of the center of mass energy for the parton system;
- x_{\min} is the minimum momentum fraction allowed. For charm, $x_{\min} = 4m_c^2/s$;
- $\sigma_{pp \rightarrow c}$ is the short distance parton-charm cross section.

Most charm cross sections are calculated for hadrons incident on individual protons or neutrons, while most experiments use targets with complex nuclei. A method for converting cross sections from a nucleonic to a nuclear level must be developed, otherwise the cross section must be measured directly. Adding complexity is that the structure functions of nucleons change when inside a nucleus; this is called the EMC effect. [3] At low x ($x < 0.1$), the ratio of structure functions of a nucleon inside a nucleus to that of a free nucleon:

$$\frac{A^{-1}F_2^{\text{Nucleon}}}{F_2^{\text{Free}}} < 1.0. \quad (2.2)$$

This leads to the *shadowing* of nucleons within the nucleus, i.e. the cross section of hadron-nucleus interactions are lower than predicted if the hadron-nucleon cross sections

are scaled up by a factor of A . The nucleons within the nucleus appear to be blocking the incident hadrons from interacting with the nucleons behind them.

It would be unwieldy to use a different structure function for each target nucleus, therefore the cross sections are determined for a single nucleon and modified to the nuclear level by the A -dependence parameter α . The nuclear cross sections are parameterized by:

$$\sigma = \sigma_0 \cdot A^\alpha, \quad (2.3)$$

where:

- σ is the nuclear cross section.
- σ_0 is the nucleonic cross section.
- α is the A -dependence parameter which varies from $2/3$ for hard sphere scattering to 1 for volume dependent scattering.

In the production of heavy quark flavors, the value of α depends upon the beam energy that determines the energy fraction, x , of the interacting parton. For the E769 experiment, with a beam energy of 250 GeV, the prevailing value of x was ~ 0.2 , therefore one would expect a higher value for the E791 beam of 500 GeV. This would indicate that the value for α should be close to 1. Also, at large x_F the value of α will be diminished because of the change in the parton distribution curve. This effect should not be present in the E791 data due to an inefficiency in the center of the drift chambers, called the 'DC hole', which limits the value of x_F to values from -0.1 to ~ 0.4 .

The calculation of the cross sections for the pion beam incident on the target is a lengthy one beginning with the basic formula of the production of x type particles from pions [2] :

$$\sigma_{\pi \rightarrow x}^N(i) = \frac{N_{\pi \rightarrow x}(i)}{N_{\pi}(i)} \cdot \frac{A_i}{\rho_i N_A t_i}, \quad (2.4)$$

where:

- $\sigma_{\pi \rightarrow x}^N(i)$ is the per nucleus cross section of producing x particles from target i ;
- $N_{\pi \rightarrow x}(i)$ is the total number of events containing x coming from target i ;
- $N_{\pi}(i)$ is the total number of pions at target i ;
- A_i is the atomic weight of target i ;
- ρ_i is the density of target i ;
- N_A is Avogadro's number;
- t_i is the target thickness in cm.

After a lengthy derivation the cross section formula for pions on a target of type i that creates D^0 mesons is given by [2] :

$$\sigma_{\pi \rightarrow D^0}^N(i) = \frac{1}{BR(D^0 \rightarrow K^- \pi^+)} \cdot \frac{A_i}{\rho_i N_A t_i} \cdot \frac{1}{R_{\pi} T_{\pi}(i)} \cdot \frac{n_{\pi \rightarrow D^0 \rightarrow K\pi}(i)}{\epsilon_{\pi}(i)}, \quad (2.5)$$

where:

- i is the index for the target type (Pt or C);
- A_i is the atomic number of the target;
- ρ_i is the density of target i ;
- N_A is Avogadro's number;
- t_i is the target thickness in cm;
- R_{π} is the pion beam fraction reaching the first target;

- $T_{\pi}(i)$ is the amount of beam reaching target i from the first target;
- $BR(D^0 \rightarrow K^- \pi^+)$ is the branching ratio for $D^0 \rightarrow K^- \pi^+$;
- $n_{\pi \rightarrow D^0 \rightarrow K^- \pi^+}(i)$ is the $D^0 \rightarrow K^- \pi^+$ signal from target i ;
- $\epsilon_{\pi}(i)$ is the total efficiency (detector and reconstruction) for finding events from target i .

The number of events observed in a given decay mode is proportional to the luminosity of the beam, the nuclear cross section, the branching ratio of the mode, and the total efficiency, giving:

$$N_{\text{OBS}} = \int L dt \cdot \sigma \cdot BR \cdot \epsilon_{\text{TOTAL}}, \quad (2.6)$$

where:

- $\int L dt$ is the integrated beam luminosity.

The luminosity is defined as:

$$L = \frac{I_0 \cdot \rho \cdot N_A \cdot \Delta z}{A}, \quad (2.7)$$

where:

- I_0 is the incident beam rate;
- ρ is the target density;
- A is the atomic number of the target;
- Δz is the target thickness;

- N_A is Avogadro's number.

Using the A-dependence formula (2.3) cross section and taking the ratio of the number of the platinum and carbon cross sections;

$$\frac{\sigma_{Pt}}{\sigma_C} = \left(\frac{A_{Pt}}{A_C} \right)^\alpha. \quad (2.8)$$

Substituting (2.5), (2.6), and (2.7) into equation (2.8), eliminating common factors such as the branching ratios and beam fractions, and solving for α :

$$\alpha = \frac{\ln \left(\left(\frac{N_{Pt}}{N_C} \right) \cdot \left(\frac{\rho_C}{\rho_{Pt}} \right) \cdot \left(\frac{A_{Pt}}{A_C} \right) \cdot \left(\frac{\Delta Z_C}{\Delta Z_{Pt}} \right) \cdot \left(\frac{\epsilon_C}{\epsilon_{Pt}} \right) \right)}{\ln \left(\frac{A_{Pt}}{A_C} \right)}, \quad (2.9)$$

where:

- $N_{Pt,C}$ are the number of events observed in the platinum and carbon targets;
- $\left(\frac{N_{Pt}}{N_C} \right) \cdot \left(\frac{\rho_C}{\rho_{Pt}} \right) \cdot \left(\frac{A_{Pt}}{A_C} \right) \cdot \left(\frac{\Delta Z_C}{\Delta Z_{Pt}} \right) \cdot \left(\frac{\epsilon_C}{\epsilon_{Pt}} \right)$ shall be called the 'corrected ratio'.

Equation 2.9 is a remarkably simple, due to the cancellation of most of the more esoteric and hard to measure terms. There are only two variables, the number of observed events in the target and the efficiency of finding events in that target. The rest of the parameters in the equation are constants such as the density and atomic number of the target. This allows quick determination of the A-dependence.

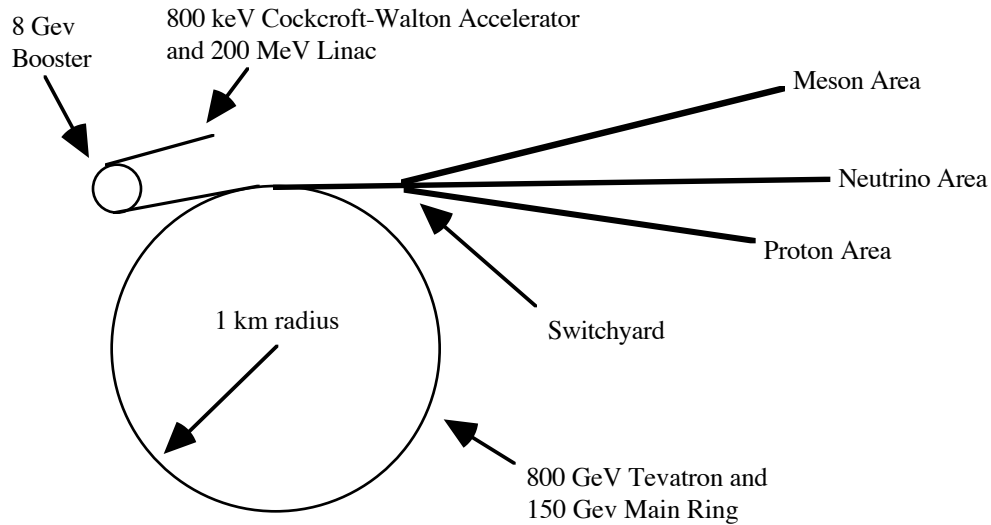
Chapter Three: The Fermilab Tevatron and the E791 Spectrometer

The Fermilab Tevatron

The Fermi National Accelerator Laboratory's 800 GeV/c Tevatron produced the protons that created the pion beam used in E791. There are five stages to beam production in the Tevatron. First, hydrogen ions (H^-) are produced by passing neutral hydrogen over a cesium source, adding an electron to the atom. The ions are then accelerated by a Cockcroft-Walton accelerator to an energy of 750 keV and injected into the LINAC. Second, the LINAC accelerates the H^- beam to 200 MeV and bunches the beam into buckets with a 19 ns spacing. The ions are then stripped of both electrons and passed to the third stage 8 GeV booster ring. The beam intensity is approximately 35-40 mA before booster injection. The booster injects the buckets into the 150 GeV Main Ring. In the final stage, the 150 GeV protons are injected into the Tevatron that accelerates the beam to an energy of 800 GeV. The entire process takes about 34 seconds and results in $\sim 2 \times 10^{13}$ protons orbiting in the Tevatron. [4]

The booster and main ring use conventional magnets to bend the particle trajectory, while the Tevatron uses superconducting magnets. The beam was extracted to the various experimental areas during a 23 second spill in the switchyard area. The length of this spill increased the time between interactions, allowing the experiment to record the data from the detectors.

Figure 2
Layout of Accelerator and Beamline System.



Beam

The beam used in the E791 experiment at the Tagged Photon Lab consisted of 500 GeV/c negative pions (π^-). These pions were generated from the interaction of 1.2×10^{12} 800 GeV/c protons/spill with an upstream beryllium target of 30 cm thickness in the Proton Area. [2] The resulting particles were momentum filtered by a dipole magnet and collimated to produce the 500 GeV/c beam of pions. This beam was recollimated and focused by quadrupole and dipole magnets before striking the experiment target to produce a narrow, parallel stream of negative pions. The beam rate for the experiment was 2 million pions per second. [5]

The Tagged Photon Lab Spectrometer

The spectrometer at TPL has been used for many years in the study of particle physics. Previous experiments such as E691 and E769 have focused on heavy quark physics. The spectrometer has undergone many changes over the years, but the primary layout has remained constant.

The spectrometer used a fixed target and had multiple detectors, including SMD planes, drift chambers, PWC planes, and Cerenkov counters. Major changes were made to the spectrometer after the E769 data run to improve tracking efficiency and increase the data acquisition rate. A schematic of the spectrometer is shown in Figure 3.

Beamline PWC & SMD

Before striking the experiment target, the beam passed through a series of Proportional Wire counters (PWC) and Silicon Microstrip Detectors (SMD) to track the beam position. This tracking was vital to the determination of the position of the primary interaction vertex inside the experimental target in the transverse X and Y directions, where Z is in the beam direction. There were a total of eight planes of PWCs and six planes of SMDs, an upgrade of four planes from the previous experiment, E769, at TPL. [5]

Figure 3
The TPL/E791 Spectrometer

Experimental Target

The E791 target consisted of five target foils arranged coaxially in a Plexiglas holder that held the foils at a precise separation. The foils were of two different elements, one platinum foil and four carbon (diamond) foils, and were of different thicknesses, 0.5 mm for the Pt target and 1.6 mm for the C targets. The beam pions interacted with the target foils to produce the charm particles. The thinness of the targets allowed precise measurements of the primary vertex Z position while the separation between the targets created sufficient volume to cleanly reconstruct the secondary vertices. The targets allowed 0.4 % of the incident pions to interact in each target. An important consideration was the choice of target material which allowed a measurement of the relation between the charm cross section and the atomic number of the target. Therefore, materials with widely different atomic numbers were selected, 195 and 12 respectively.

Table 2
Target Information

Target Number	1	2	3	4	5
Target Type	Platinum	Diamond	Diamond	Diamond	Diamond
Atomic No.	78	6	6	6	6
Atomic Wt.	195.08	12.01	12.01	12.01	12.01
Thickness (cm)	0.052	0.1572	0.1567	0.1530	0.1544
Diameter (cm)	1.606	1.369	1.377	1.368	1.355
Mass (grams)	2.2396	0.7490	0.7507	0.7373	0.7300
Density (g/cc)	21.3	3.24	3.22	3.28	3.28
Radiation Length	0.169 (Target) 6.54 (Material g/cm ²)	0.012 42.70	0.012 42.70	0.012 42.70	0.012 42.70
Proton Interaction Lengths	0.00584 (Target) 189.7 (Material g/cm ²)	0.00590 86.3	0.00585 86.3	0.00582 86.3	0.00587 86.3

The carbon targets were synthetic diamonds normally used for oil well drill bits and were purchased from General Electric Superabrasives. [6] The diamonds include about 6% air by volume and may contain up to .5% Cobalt. The platinum was 99.95% pure and certified by the government of Australia.

Trigger

The E791 experiment used a very loose trigger, allowing the spectrometer to record a large quantity of data. A loose transverse energy component (E_T) cut, as measured by the electromagnetic and hadronic calorimeters, was applied to increase the likelihood of detecting charmed particles. The decay of charmed particles creates events in which the decay products have a larger amount of transverse energy and momentum than in light quark particle decays. Also, events were rejected if two beam particles were in coincidence, as these might fake a high transverse energy event, thereby passing through the E_T cut. [5]

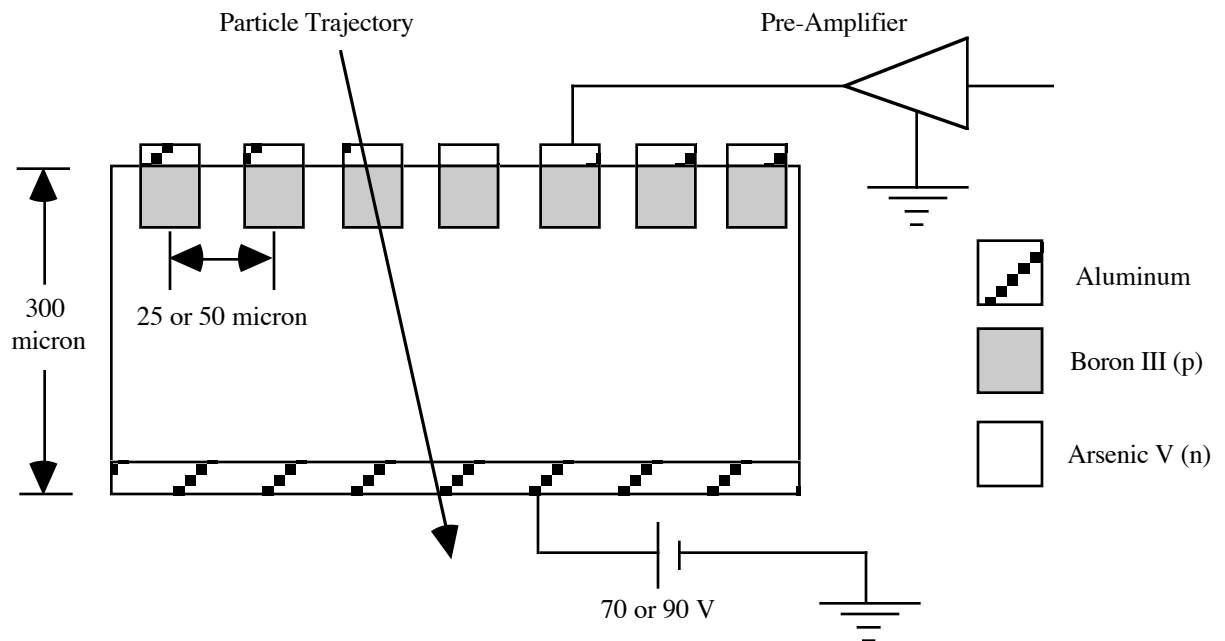
Downstream SMD

The Silicon Microstrip Detector (SMD) plane system was of primary importance in the tracking of the decay particle tracks. The SMD system tracked the flight of the decay products close to the target and achieved a high resolution due to the narrowness of the SMD strips. [7] Also, the high efficiency of the SMD system greatly enhanced the particle tracking of the spectrometer. To increase the tracking and reconstruction efficiency six new planes were added for E791 bringing the total number of downstream planes to seventeen.

There were three different orientations of SMD planes, X, Y, and V, where the V planes were rotated 20.5 degrees with respect to the vertical X-axis.

An SMD plane consisted of a 300 micron thick sandwich of aluminum strips, arsenic and boron doped silicon, and an aluminum base that creates a reverse p-i-n type diode. When a charged particle passes through the SMD plane it produces approximately 25,000 electron/positron hole pairs in the electron deficient silicon region. [2]

Figure 4
SMD schematic



The electron holes drift towards the p-type boron and are collected by the surface aluminum strips due to the potential difference across the plane. The aluminum strips on the surface are kept at 70 to 90 volts potential difference with respect to the Al base depending on the plane. There were two different plane configurations, one with 25 micron spacing from the center of each strip and the other with 50 micron spacing. The two configurations

have efficiencies of $\sim 70\%$ and $\sim 92\%$ respectively, the 25 micron planes being less efficient due to electronic and noise limitations. [4]

Downstream PWC

Additionally, two downstream planes of Proportional Wire counters (PWC) were used to increase the Y-direction track resolution and for tracking redundancy. The PWCs operate in much the same manner as the drift chambers, collecting the electrons produced when a charged particle ionizes the chamber gas. The gas used in the PWC was a mixture of 83% Ar, 17% CO₂, and 0.3% Freon. The spacing between the wires was 2 mm, producing a resolution of 600 microns.

Drift Chambers

The drift chamber (DC) system at TPL was used to track the flight of the decay products of the charmed particles as they moved through the spectrometer. Thirty-five planes of sense wires were distributed through seven separate gas boxes and four DC modules. The first module (D1) was located in front of the first analysis magnet (M1), the second module (D2) was located between M1 and the second analysis magnet (M2), the third module (D3) was located after M2, and the fourth module was located after the second Cerenkov counter (C2). In each chamber the assemblies contained different numbers of sense wire planes, four in D1 and three in D2, D3, and D4. The number of sense wires in each plane varied from 96 to 256. (See Table 3 for DC specifications.) The orientations of

the sense planes were in the X, U, and V directions, where the U and V sense planes are at an angle of $\pm 20.5^\circ$ with respect to the vertical X-axis. (See Figure 5.)

Table 3
Drift Chamber Specifications [2],[4]

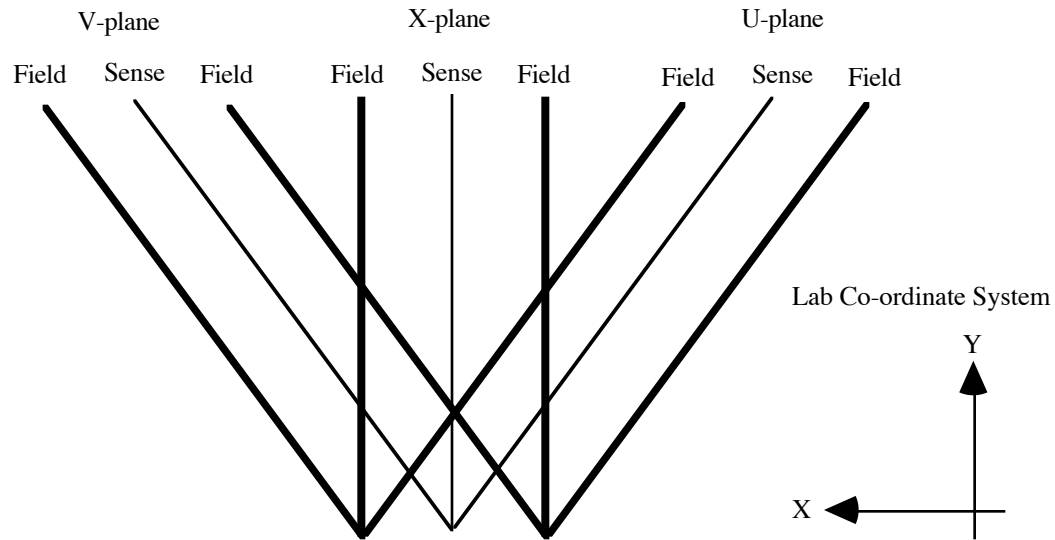
chamber	D1	D2	D3	D4
Assemblies	2	4	4	1
Planes per Asmb.	4	3	3	3
Plane Order	UVXX'	UVX	UVX	UVX
Asmb. Area	0.91 m ²	3.9 m ²	4.6 m ²	13.3 m ²
Avg. Wire Sep.	0.46 cm	0.93 cm	1.5 cm	3.0 cm
Wires per plane	96, 192, 256	176, 192, 208, 224, 240	160, 192	128, 160

Also, two X planes in D1 were offset a half cell width to define a new plane labeled X'. The X' planes aided in resolving left-right ambiguities in track finding and aid in track separation. These planes were located in the center section of D1 because of the high particle flux in that area.

A drift chamber plane consisted of three planes of wires, two planes of high voltage cathode wires and one plane of sense wires and field shaping wires. The sense wires were 25 micron gold plated tungsten while the HV wires were 127 or 125 micron Be-Cu. The HV planes were held at about -2.4 kV while the field shaping wires were at about -2.0 kV. The sense wires were grounded. Adjacent planes of sense wires in the same assembly shared the HV plane between them.

Figure 5

Drift Chamber Wire Plane Orientation



When a charged particle passed through a drift chamber it ionized the gas in the chamber. In E791 the gas used was a non-flammable mixture of 89% argon, 10% carbon dioxide, and 1% CF_4 . [5] The electrons produced are then collected by the sense wires due to the field produced by the negative HV and field planes. The signal collected is then amplified and passed through a discriminator, allowing adjustments of the signal to noise ratio.

Magnets

The two analysis magnets, M1 and M2, were located between D1 and D2, and D2 and the first Cerenkov detector (C1), respectively. The magnetic field in each magnet was oriented in the vertical direction. The magnets gave incoming charged particles a transverse

momentum (p_T) kick according to the Lorentz force law. This transverse kick, when combined with the drift chamber tracking, provided information about the particle's momentum and charge. The magnets were operated at 2500 (M1) and 1800 (M2) Amps and provided a p_T kick of -212.4 MeV/c and -320.7 MeV/c. [4]

Cerenkov Counters

The threshold Cerenkov detectors were used for particle identification; collecting the light produced by particles moving above the speed of light in the counter gas. The detector gases were chosen to increase the efficiency of identification over the wide range of possible particle momenta. The upstream detector (C1) was filled with pure nitrogen, while the downstream detector (C2) was filled with an 80% helium and 20% nitrogen mixture, and both detectors were held at atmospheric pressure. The phototube faces in C2 were flushed with nitrogen to prevent helium from penetrating the PMT window and damaging the tube. The threshold counter momenta are given in Table 4.

Table 4
Cerenkov Chamber Particle Momentum Thresholds [2],[4]

Particle Type	C1 Momentum Threshold (GeV)	C2 Momentum Threshold (GeV)
π	5.35	10.5
K	18.7	37.2
p	35.5	70.7
e	0.0193	0.0385
μ	4.01	7.99

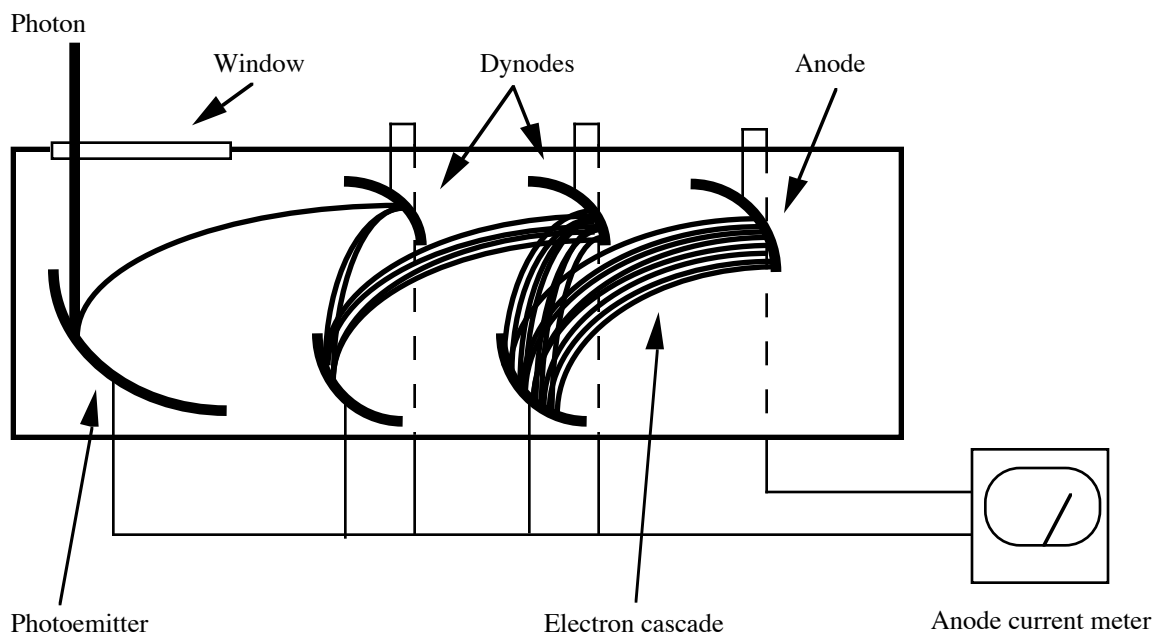
The gas mixture in C2 was measured using a Sonic Wave Monitor (SWM) system and monitored using the Low Voltage Monitoring (LVMON) system. The SWM

measured the speed of sound in a cylinder filled with gas pumped in from the C2 detector. [8] This speed was converted to a DC voltage and was calibrated via a reference source of 80/20 He/N₂ to determine the nominal output voltage. The LVMON system then read out the voltage and recorded it for future reference. The C2 gas mixture was also monitored periodically using a mass spectrometer.

The LVMON subsystem was responsible for monitoring all the low voltage power systems in E791. There were 192 channels of readouts ranging from the SMD, C1 and C2, DC, to the Exabyte tape drive power supplies. Each channel was read out through an analog-to-digital converter (ADC), with a possible range of 0 to 10 Volts or -5 to +5 Volts. Six ADC modules were used. The ADCs were then latched in the middle of the beam spill, since some detector power supplies would vary depending on the presence of beam, and readout via the CAMAC crate system. [9] The CAMAC readout was controlled by the LVMON computer program that compared the readout voltage to the voltage standards file. If the detector voltage was outside of a preset limit, the program would display a warning message in the TPL control room. The voltages would then be written approximately once per hour to a disk file on the TPL VAX 11/780.

There were 32 Photomultiplier Tubes (PMT) in C1 and 28 in C2. The incoming photons in each detector were reflected by mirror planes into Winston light collecting cones in front of each PMT face. In C1 two planes of mirrors were used to reflect the incoming light to compress the chamber and allow it to fit between the analysis magnets. Also, light baffles were installed in C1 to block Cerenkov radiation produced by beam particles passing through the detector.

Figure 6
Photomultiplier Tube Schematic



The proximity of C1 to the M1 analysis magnet produced minor problems. The central field produced by M1 was on the order of 10,000 Gauss, and produced a small, but not negligible field, in the vicinity of the PMTs. [10] The field affected the efficiency of the tubes by affecting the path taken by the electrons cascading from the dynodes to the anode and reducing the number of electrons that reached the anode. [11] To eliminate this effect the tubes were shielded with iron and mu-metal shields. This was determined to be insufficient; therefore each tube was wrapped in a bucking coil. These coils produced an opposing magnetic field when a current of sufficient magnitude was supplied. However, determining the correct current to be supplied proved to be difficult. Various methods were tried to determine the correct current by examining the tube efficiency, the single photo-electron peak (SPEP), and using a laser to measure the tube response. Finally, the brute force method was used; measuring the magnetic field at the tube face directly with a Hall Probe and adjusting the bucking coil current to reduce the field as much as possible. It was

determined that the magnetic fields produced by M1 were on the order of a few to ten gauss, which is sufficient to alter the PMT response if the bucking coils were not present.

SLIC and Hadrometer

The Segmented Liquid Ionization Calorimeter (SLIC) and the Hadrometer were used to measure the energy of the decay particles produced in the experiment. [12] The SLIC was designed to detect particles that primarily interact through electromagnetic processes, although some hadronic reactions were also detected. The Hadrometer was designed to detect hadronic processes only, and was important for the detection of neutral hadrons. Both detectors were also used in the experiment trigger and in the detection of electrons and neutral pions.

The SLIC consisted of 60 layers in the beam direction and was oriented in three directions, U, V, and Y, using the standard convention. Each layer is composed of a radiator-scintillator pair. The radiator was a 0.37 cm thick laminate of Al-Pb-Al and each laminate covered the entire area of the detector. [13] The scintillators were square corrugated, aluminum sheets forming the U, V, and Y channels of the SLIC. The channels were filled with a liquid scintillator, NE235A. The light produced reflected down the channel, due to total internal reflection, and was collected in PMTs using wavebars with wavelength shifters.

The Hadrometer was constructed of 36 radiator-scintillator assemblies, the first and last 18 assemblies grouped to form upstream/downstream sections. The radiators were ~2.5 cm thick steel plates covering the entire detector area. The scintillators were doped acrylic strips with an attached light guide. Each strip was ~14.3 cm wide and 1 cm thick.

[14] The Hadrometer sections had alternating planes of vertical and horizontal scintillator strips. In each section, the vertical and horizontal strips with the same X or Y orientation were grouped together by light guides and a common phototube.

Muon Walls

The SLIC and Hadrometer absorb most of the particles produced in the experiment, with the exception of neutrinos, muons, and a small number of hadrons. Since leptonic and semi-leptonic decay modes are of interest, information concerning the muons must be collected. To identify the muons, the hadrons which pass through the calorimeters must be filtered out. A steel wall behind the hadrometer absorbs these particles, allowing the muons through. Two walls of scintillator paddles, placed behind the steel wall, were used in E791 for the detection of muons. The passage of muons through the paddles created photons that could be detected. The paddles were made of doped acrylic with attached light guides and photomultiplier tubes. The upstream paddles were oriented in the vertical direction and the downstream paddles in the horizontal direction. The combination of vertical and horizontal walls were used to better associate tracks in the detector to muon hits in the paddles. The addition in E791 of the second wall of muon scintillator paddles made possible the observation of single muon decays of D mesons. This was not possible with a single wall.

Chapter Four: Data Acquisition System

The data from the experimental detectors was read out by various methods, including latches, analog-to-digital converters (ADC) and to time-to-digital converters (TDC). These readout systems comprised the beginning of the Data Acquisition (DA) system. The digitizers, the number of channels per system, and the fraction of tape each system wrote are recorded in Table 5.

The main goal of E791 was to collect a large charm particle sample. To accomplish this a loose trigger system was designed allowing many events to be accepted. The percentage of accepted events, the high beam rate, and a new DA system increased the data sample by a factor of ~40 over the previous experiment. Therefore, the DA system needed to digitize and record at an extremely high rate due to the large number of events and the large number of data channels, 24,000. All channels in the detector were read out in 50 microseconds, another requirement due to the high beam rate. All the data from the detectors arrived during the 23 second spill but was stored and written to tape continuously. Large Event FIFO Buffers (EFB) allowed the data to be stored during the 34 second interspill. Without this interspill data writing, the DA system would not be able to handle the large quantity of data. The data arrived at a rate of 26 Mbytes/sec but was written to ~42 8mm Exabyte tape drives at a rate of 9 Mbytes/sec. [15]

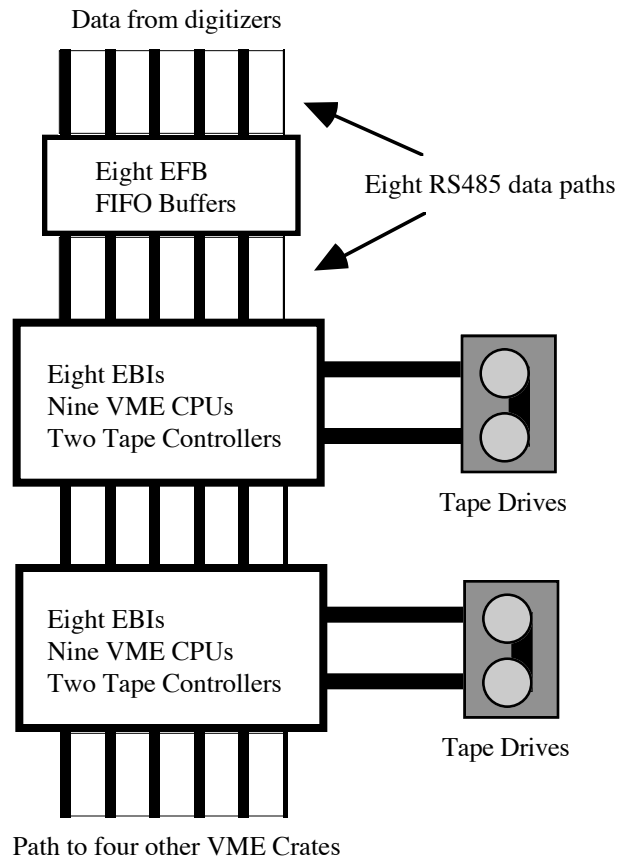
The data from each individual event passed along eight separate RS485 32-bit wide data paths. Each detector passed data through a specific data path to an Event FIFO Buffer (EFB) containing 80 Mbytes of DRAM and held that data until the VME crates called for it.

Table 5
Data Acquisition System [15]

System	drift chambers	Cerenkov & Calorimeter	SMD	PWC	CAMAC
Digitizer	Phillips TDC	LeCroy FERA ADC	KSU & Nanometric Latches	LeCroy Latch	LeCroy Latch, PLU & Scaler
Channels per system	6304	554	15896	1088	80
Tape fraction	50%	27%	18%	3%	2%

There were six VME crates each containing eight Event Buffer Interfaces (EBI), nine VME CPU cards, and two tape drive controllers. (See Figure 7.) The VME crates reassembled each event from the eight parts contained in the EFBs, this process was called 'munching' the event. When one VME crate was busy munching an event the next crate in the chain would begin munching its own event. During this process the data were compressed to allow more events to be written to tape. Once this process finished, the data were passed to the 8mm Exabyte tapes drives. Each of the six VME crates could write events to seven different tape drives at 0.25 Mbytes of data per second each, making an overall write speed of ~10 Mbytes/s. In the course of the 1991 run, 20 billion data events were written to tape, using 24,000 8mm tapes with an overall data set of 50 Terabytes. [15]

Figure 7
The Data Acquisition System



Chapter Five: Data Reconstruction

After the data collecting run was completed, there were about 24,000 data tapes to be analyzed. To accomplish this task large computer 'farms' were assembled at The Ohio State University and at The University of Mississippi. [16] Each farm was composed of a large number of independent computers linked through Ethernet and totaling ~1000 MIPS (Millions of Instructions Per Second) of computing power. Event processing began in February 1991. Additional farms were constructed at Fermilab and the Centro Brasileiro de Pesquisas Fisicas; the Ohio farm was moved to The Kansas State University; and the Mississippi and Kansas farms underwent substantial upgrades. The Mississippi computers utilized were Digital Equipment Corporation's DECstation 5000/200 with 25 MHz MIPS R3000 RISC CPUs and the DECstation 5000/50 with 50 MHz MIPS R4000 RISC CPUs running the ULTRIX operating system. The Mississippi farm was divided into chains each with independent job managers and a series of client computers. The job manager read out blocks of events from the data tape and passed one block to each of the client computers, which then analyzed the events using the E791 analysis package. The client computer then wrote the reconstructed event to a disk file. The disk files were later moved to a Data Summary Tape (DST). After completing one block of data, the client was ready to accept a new block from the job manager. In this manner each farm operates as a loosely coupled parallel processing system.

The reconstruction or filter program analyzed each event by attempting to link hits in the various detectors into particle tracks and extracting 4-vector momentum from those

tracks. The program consists of various smaller subroutines, each with a specific task. A large portion of the program was concerned with finding particle tracks in the detector, a track being defined by hits in various detector channels which form a continuous line in three dimensions. There were two main track subroutines, ESTR (Exhaustive Search Track Reconstruction) and SESTR (Silicon ESTR) performing similar tasks. SESTR examined the tracks in the SMD system. It attempted to form straight line tracks in the SMD planes and then project that track through the rest of the spectrometer. The projected track can either be straight or bent, depending on the co-ordinate involved. In the horizontal X direction, a charged particle track can be bent by the analysis magnets, while it must be straight in the vertical Y direction. SESTR attempted to connect all tracks in the SMD planes to tracks in the drift chambers. Once completed, SESTR used the bending caused by the analysis magnets to determine the particle momentum. ESTR operated in the same manner, but using only left over DC tracks, i.e., tracks not associated with SMD tracks as found by SESTR. Some particles, such as lambdas and K-shorts, will decay after passing through the SMD system, producing tracks only in the DC. ESTR finds these tracks and the associated momenta.

Once the co-ordinates, charge, and momentum of each track was determined, the data from the other detectors were examined. One of the more important parts of the analysis was the determination of the parameters concerning the primary and secondary vertices. The VTXSTR subroutine was the primary vertexing package. It determined if two or more SMD tracks formed a vertex and the parameters of that vertex, such as its co-ordinates and positional error. In the Cerenkov counters, hits in the PMTs were associated with tracks passing through the mirror planes and used in particle type identification. The tracks were then projected through the calorimeter to associate tracks with channel hits to

measure the particle energy. The muon wall was used to identify tracks as muons. The data were then packaged into the DST format and passed back to a job manager to be written to tape.

The reconstruction of an entire run of raw data tapes, usually ~40, produced about 12-14 DST output tapes. These tapes are copied and sent to the various collaborators on the experiment for analysis and stripping.

Chapter Six: Stripping the D Meson Signal From the DST Tapes.

Once the DST tapes are written, the relevant information must be extracted about the particular particle or decay mode of interest via stripping. This stripping involves further analysis of the data on the DST and comes in two basic forms, vertex-list or candidate driven. In a vertex-list driven strip, each event is examined by looking at the vertices formed by the intersection of two or more particle tracks. The DST contains a list of the primary and secondary vertices and the strip examines each vertex in the list determining various parameters that signal the presence of certain particles or decays. A candidate driven strip examines the particles involved in each event and attempts to find the desired decay mode by tracing the particles that give the correct mass to a common vertex. The candidate driven approach allows greater flexibility since new vertices can be found that are not on the vertex list, but is more difficult to implement. The D meson strip used the vertex-list approach due to the complexity of the candidate driven method.

The D meson strip was a three part strip, using the multi-stream output (MSO) stripper and two smaller related strips. The MSO stripper examined the DST tapes and could run up to twenty different stripping subroutines simultaneously, writing both to tape and disk files. Various strip subroutines such as a three-prong vertex, p - K - π , K - π , and K - π - π were installed. Each subroutine was designed by various experimenters and usually used minor cuts to extract the relevant signal. The K - π and K - π - π strip subroutines were based on my original strips and updated for faster processing and to correct programming

errors. The MSO strip was designed as a tool for multiple experimenters to extract data from DST tapes.

The smaller related strips used almost identical subroutines as the MSO subroutines except for tighter cuts, additional histograms, and additional code to determine target data. The first related strip used was a data cut strip. It applied tighter data cuts to the events extracted from the MSO data. It produced an output strip tape to be analyzed by the final stripping routine. The third strip examined the events for data concerning the position of the primary interaction vertex in relation to the target position. Each strip used the E791 off-line processing shell that is used to read the data tapes, unpacks the events, and write the histogram and output data to tape or disk. The off-line shell also called the various stripping subroutines that created and filled the histograms and examined the events. The stripping subroutines were named `kpi_st_cut.f`, `kpi_st_tgt.f`, `kpipi_st_cut.f`, and `kpipi_st_tgt.f`, where the 'cut' subroutines were called by one strip and the 'tgt' routines by the other.

DST stripping proceeded as follows:

- 1: DST tapes were stripped by the MSO stripper to disk and tape files.
- 2: The $K-\pi$ and $K-\pi-\pi$ disk files were dumped to tape.
- 3: The combined $K-\pi$ and $K-\pi-\pi$ tape was stripped by the cut strip program and written to tape.
- 4: The cut-stripped $K-\pi$ and $K-\pi-\pi$ tape was examined by the target strip program. The program generated a histogram file from which the target data were extracted.

In this manner 39 runs were examined for $D^0 \rightarrow K-\pi$ events and 40 runs were

examined for $D^+ \rightarrow K\pi\pi$ events. The amount of data examined represented one-fifteenth of the data collected by E791 during its data taking run.

The cuts used by the stripping routines were determined by examining the signal-to-noise ratios of various sets of cuts while maximizing the number of events with the mass of the D meson. Also, a small study was made of the effect of adjusting various cuts. The TGTF cut appeared to have no effect on the data and might result in an inaccurate measurement. The cut was therefore removed, although the possibility of replacing the TGTF cut was left open. The chosen set of cuts, listed below in Table 6, was similar to the cuts used by the KSU stripping programs.

Table 6
Cuts Used in D Meson Stripping

D^0 Cuts

Cuts Name	Cut Value
SDZ	> 8.0
TAU	< 2.0 ps
PRA	< 0.75
PTB	< 0.35 GeV
Mass Window	$1.7 < \text{Mass} < 2.1$ GeV
CPRB2	> 0.16
TGTF	0^2

D^+ Cuts

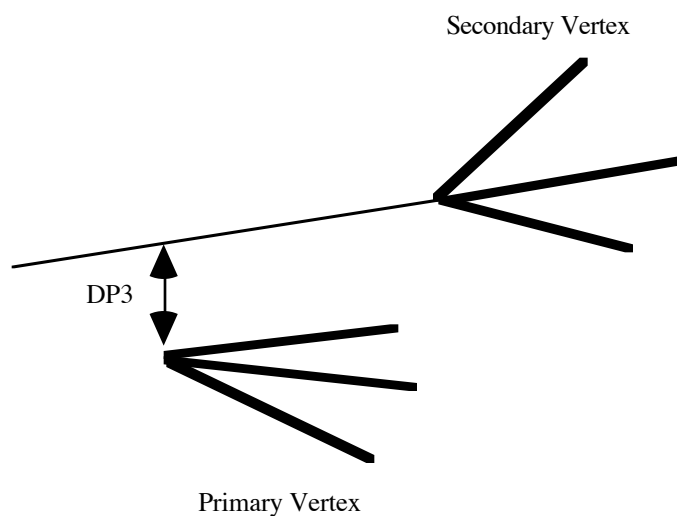
Cut Name	Cut Value
SDZ	> 6.0
TAU	< 5.0 ps
DP3	< 0.02 cm
Mass Window	$1.7 < \text{Mass} < 2.1$ GeV
Kaon Probability	> 0.15
Pion Probability	> 0.10

²Originally cut was set to TGTF > 0.1 cm, but was later changed. See text for more details.

The cuts are defined as follows:

- SDZ: the Z separation of the primary and secondary vertices divided by the error in separation.
- TAU: proper lifetime cut for particle.
- PTB: the transverse momentum difference of the two tracks with respect to line joining primary and secondary vertices
- PRA: decay asymmetry $PRA = \frac{p_1 - p_2}{p_1 + p_2}$ where p_1, p_2 are the momentums of the two particles.
- CPRB2: probability of particle being a kaon.
- DP3: impact parameter. See Figure 8.
- Mass Window: removes data far from mass peak.
- TGTF: removes secondary vertices which lie within target thicknesses.

Figure 8
DP3 Cut Representation



The number of events in each target mass peak and associated errors for the two decay modes are presented in Table 7. This number was calculated by fitting the data using a Gaussian fit for the mass peak on a linear background. Both fits were done minimizing chi-square. All mass plots in this thesis were generated using the PAW (Physics Analysis Workstation) histogramming program and utilized KUMAC files which fitted the plots. PAW also determined the error on each fit, and where background events were present, correctly determined the combined error of the linear and Gaussian fits.

Table 7
D⁰ and D⁺ Fitted Mass Plots for Each Target.

D⁰ Events

Target Number	Target Type	Number of Events in Mass Peak	Error in Number of Events in Peak
1	Platinum	506.6	43.6
2	Carbon	521.9	43.98
3	Carbon	569.0	44.1
4	Carbon	604.0	45.83
5	Carbon	638.4	47.62

D⁺ Events

Target Number	Target Type	Number of Events in Mass Peak	Error in Number of Events in Peak
1	Platinum	747.9	61.83
2	Carbon	786.1	68.53
3	Carbon	706.9	61.5
4	Carbon	686.3	61.0
5	Carbon	597.5	57.36

Figure 9
D⁰ Mass Plots

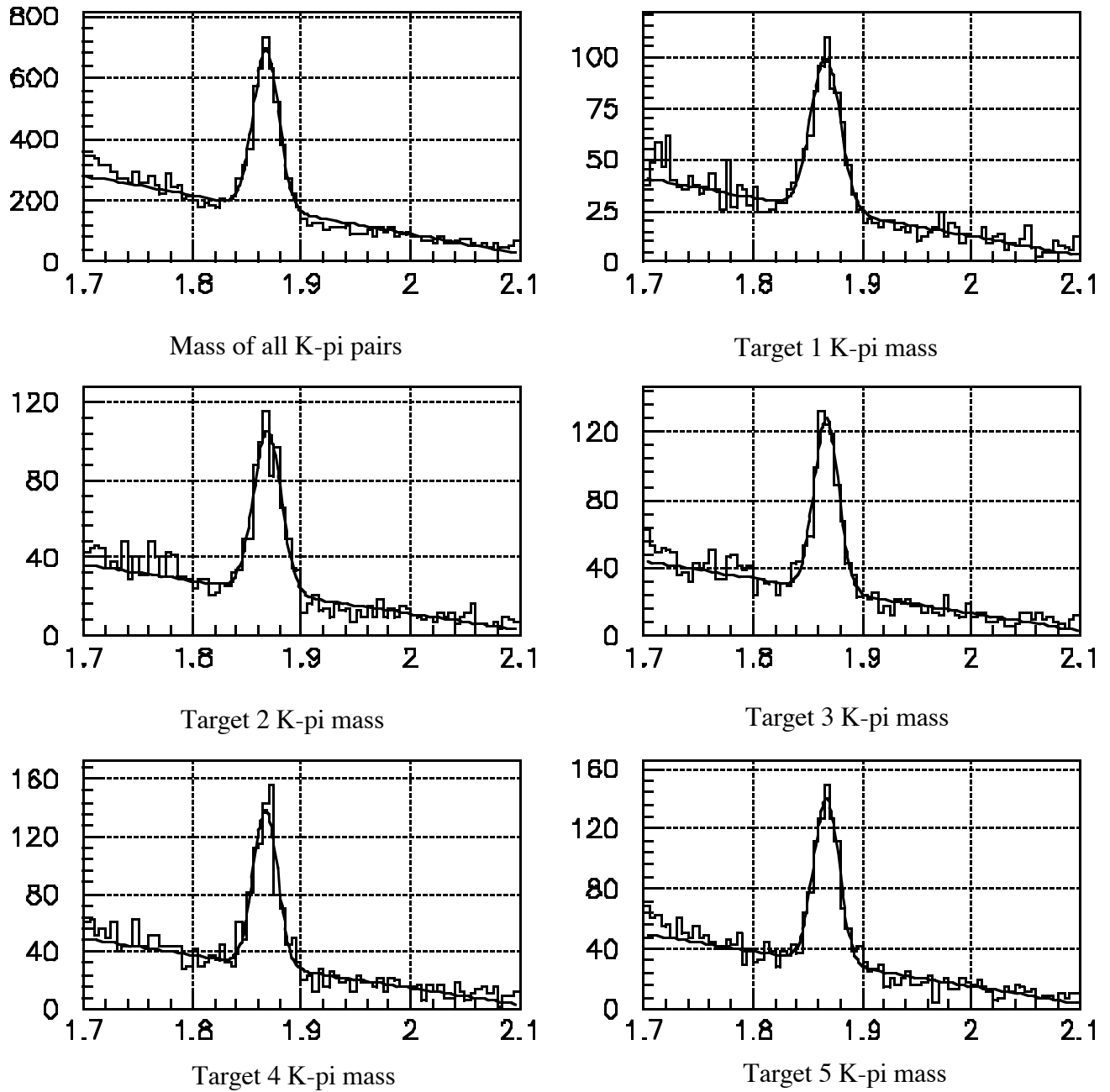
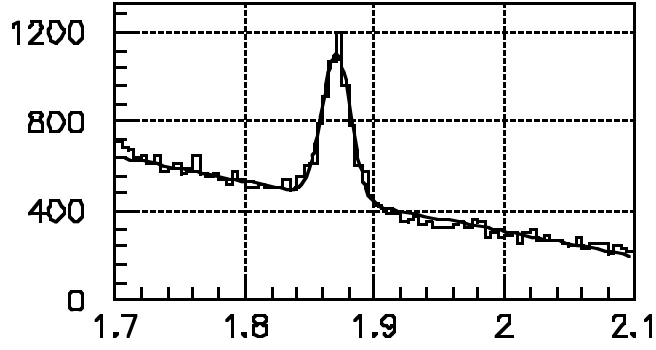
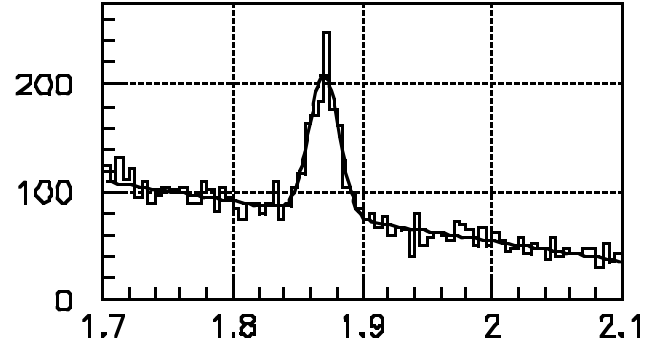


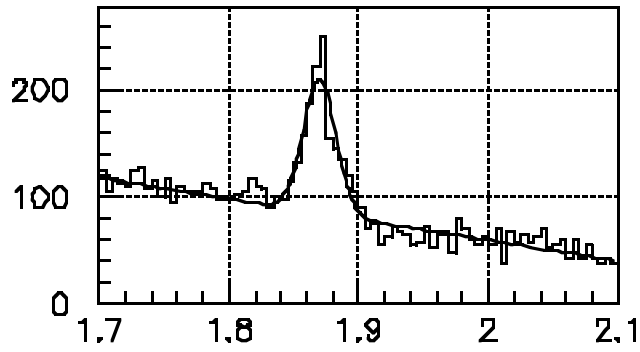
Figure 10

D⁺ Mass Plots

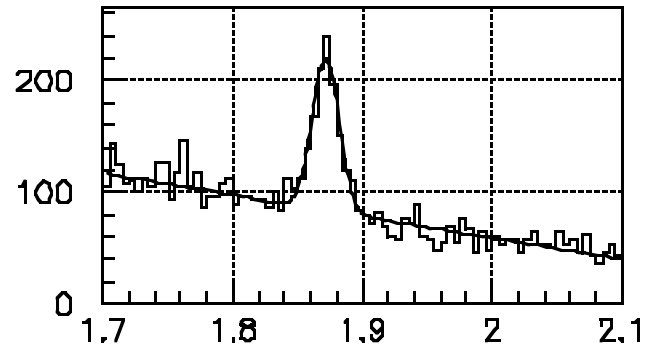
Mass of K-pi-pi triplet



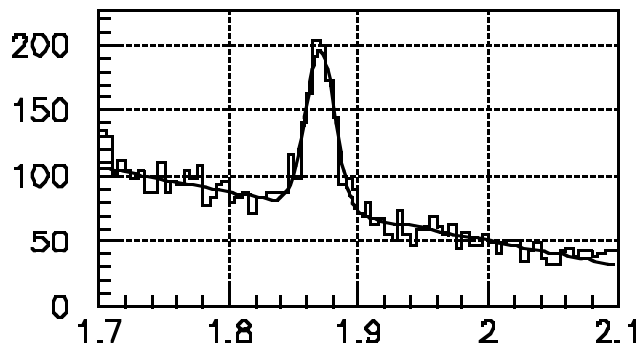
Target 1 K-pi-pi mass



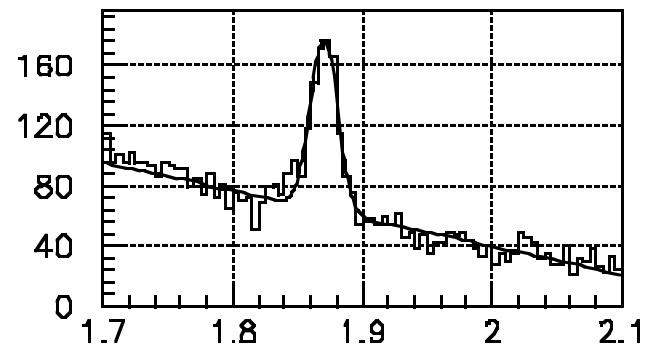
Target 2 K-pi-pi mass



Target 3 K-pi-pi mass



Target 4 K-pi-pi mass



Target 5 K-pi-pi mass

Chapter Seven: The Monte Carlo Simulation

The TPL spectrometer is a very complex device with many channels of data, planes of detectors, Cerenkov counters, and a very complex data acquisition and reconstruction system. The task of measuring the total efficiency would be virtually impossible by any physical means. Therefore, the development of computer simulations that are able to numerically model the detector and the particle interactions makes the analysis of HEP data possible. These simulations are called Monte Carlo (MC) programs. They are designed to completely model the detector, the particle interactions, and simulate the data produced in the experiment using various programs and routines.

The first package is PYTHIA. It is the generator for the MC beam particles and models the interactions between the beam and the target. PYTHIA determines which quarks are created in the primary interaction. Since quarks are not directly observable, they produce 'stable' particles that are seen by the detectors through 'hadronization'. Hadronization is not well understood, but can be modeled by observation of real interactions and some theoretical calculations. Hadronization is handled by the JETSET package that incorporates the LUND fragmentation model. The 'stable' particles are created by JETSET and their properties, such as energy and momentum, are specified. The hadrons produced are then moved through the simulated detectors making hits in various planes, light in the Cerenkov counters, and depositing energy in the calorimeters. The entire spectrometer is simulated using data files which contain information on every aspect of the systems. Position, orientation, interaction lengths, Cerenkov gas, and efficiencies are all included, and many of these data files are also used by the reconstruction

program to perform tracking, for instance. Once the event has been modeled by the MC it is converted to the E791 DST format, with one major addition. The MC adds a 'truth table' to the event record that states exactly what occurred in the event. This truth table is not used in the reconstruction, instead it is examined by a separate program which is used to compare the actual data generated by the MC to the data the reconstruction produces. In this manner the detector efficiencies can be measured.

The process for creating and using an MC tape to measure efficiencies is:

- 1: The user determines the number, particle type, and decay mode of the events that the MC will generate.
- 2: The MC program is then run generating a raw MC data tape.
- 3: The raw MC tape is processed using the reconstruction farm producing an MC DST tape.
- 4: The DST tape is run through the user's stripping routine and the data of interest is extracted, such as number of hits per target.
- 5: The raw MC tape is run through a separate program that examines the 'truth table' for each event. The actual figures for the data of interest are extracted.
- 6: The results from the stripped DST and the truth tables are compared to measure the total efficiencies.

This is the process used to make the MC tapes for measuring the D meson efficiencies. A total of 40,000 $D^0 \rightarrow K^- + \pi^+$ and 20,000 $D^+ \rightarrow K^- + \pi^+ + \pi^+$ events were generated and processed through the Ole Miss farm. The MC DST tapes were

stripped and the number of events occurring in each target were found from both the strip and from the MC truth tables. The results follow in Table 8. Note that the sum of the number of events found by the truth tables does not equal the number of events generated. This is because a fraction of the events were not generated in the target area, but in the interaction counter, a scintillator paddle in the trigger system.

Table 8
D Meson Signals for each Target as Generated by the MC.

D⁰ Events

Target	Events from Stripped DST	Error for Events from Stripped DST	Actual Number from Truth Tables
1	256.5	16.90	7540
2	279.2	17.40	7053
3	297.9	17.72	6992
4	322.4	18.81	6893
5	341.1	19.61	7230

D⁺ Events

Target	Events from Stripped DST	Error for Events from Stripped DST	Actual Number from Truth Tables
1	121.5	11.29	3875
2	120.6	9.981	3500
3	109.5	10.89	3520
4	118.3	12.90	3481
5	99.32	10.75	3551

From Table 8, the total efficiency (detector, acceptance, and reconstruction) per target can be calculated by dividing the number of events found by the strip to the actual number contained in the truth tables. Table 9 contains the combined results. It is apparent

that the efficiencies between the modes do not correlate well. The D^0 mode numbers start low and gradually increase. The D^+ efficiencies do not follow that trend; the lowest result comes in the last target, not the first. One would expect the trend seen in the D^0 figures since the detector subtends a smaller solid angle than the last target. See Figure 11 for a plot of efficiencies versus target position. The chances for an event in the first target to be completely reconstructed would therefore be somewhat lower. It appears that the D^+ MC events may not be as reliable. The differing lifetime of the D^+ partially explain this observation. The D^+ lives longer than the D^0 and therefore will travel further through the detector, occasionally decaying between the SMD planes. This would decrease the tracking efficiency for targets closer to the SMD planes.

Table 9
Total Efficiency by Target

Target	D^0 Efficiency (%)	D^+ Efficiency (%)
1	0.0340 ± 0.0022	0.0314 ± 0.0029
2	0.0396 ± 0.0025	0.0345 ± 0.0029
3	0.0426 ± 0.0025	0.0311 ± 0.0031
4	0.0468 ± 0.0027	0.0340 ± 0.0037
5	0.0472 ± 0.0027	0.0280 ± 0.0030

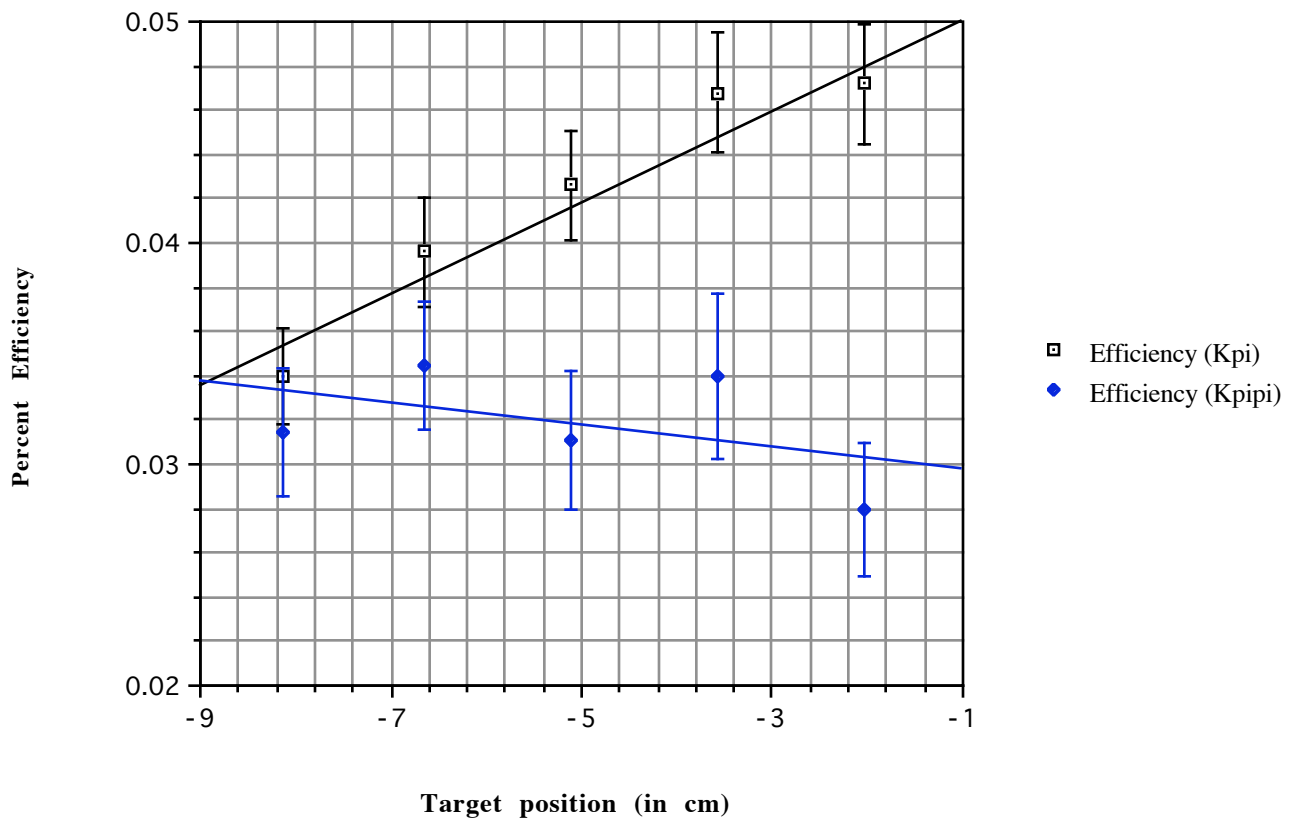
The accuracy of the Monte Carlo simulation is of vital importance in determining the detector efficiency, therefore the data from the MC was compared to the data gathered by the strip. The D^0 mode was chosen because it was the easiest studied and a large MC sample was produced early in the study. The D^+ mode was examined in far less detail, because the inconsistency in the trend of the efficiencies.

Histograms were made of various parameters for both the real and MC D^0 events and compared. The first check was the position of the primary vertex. Figure 12 shows

plots of the primary vertex positions for the real and MC data. Careful scrutiny of the data revealed that the MC target positions were not the same as the positions found in the real data. (See Table 10.) These discrepancies are small, on the order of a half millimeter, and should not directly affect the A-dependence. However, the thickness of the platinum target

Figure 11
Percent Efficiency versus Target .

Efficiency vs. Target from Monte Carlo Data



is about a half millimeter and this positional error could effect the number of events that appear to be coming from that target. The section of code that determines the primary vertex position attempts to find the target closest to the vertex. The distance between the

targets is over one centimeter and the average separation between the vertex and target center is much smaller. Therefore, there should be little signal loss due to the error in the target position data.

Table 10
Target Positions in cm

Target	MC Value	Stripper Value	From Real Data
1	-8.191	-8.123	-8.143
2	-6.690	-6.646	-6.658
3	-5.154	-5.110	-5.122
4	-3.594	-3.575	-3.584
5	-2.060	-2.036	-2.046

The next logical step is to examine the X-Y primary vertex locations. This maps the position of the target in the directions perpendicular to the beam. All five targets were circular in shape and one would expect to see circular primary vertex distributions. The MC program, however, generates elliptical distributions. (See Figure 13.) In the target data blocks, each target is defined to be circular therefore it appears that the MC is generating beam particles with an elliptical distribution. The real data was then cut to resemble this elliptical pattern to determine any effects. The number of events in each target changed somewhat but this change was uniform and did not appear to favor one target over another. The unusual MC distribution should not adversely effect the A-dependence measurement.

Figure 12
Primary Vertex Position in cm
(MC data on left , real data on right)

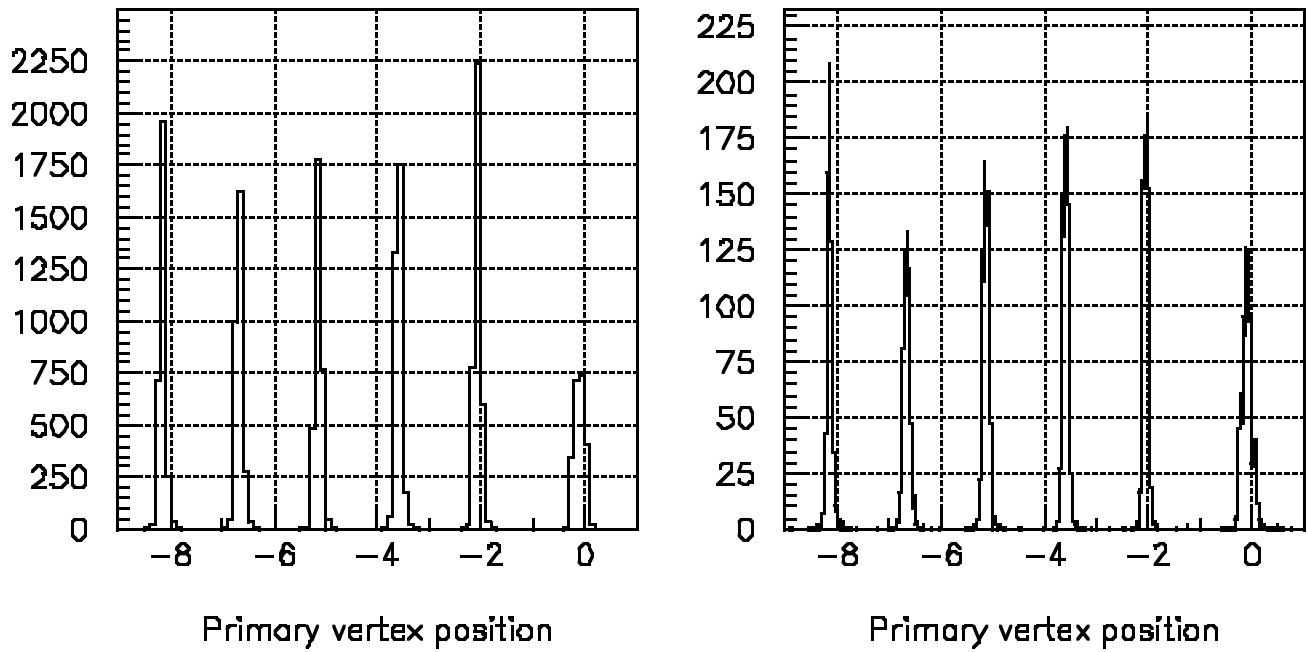
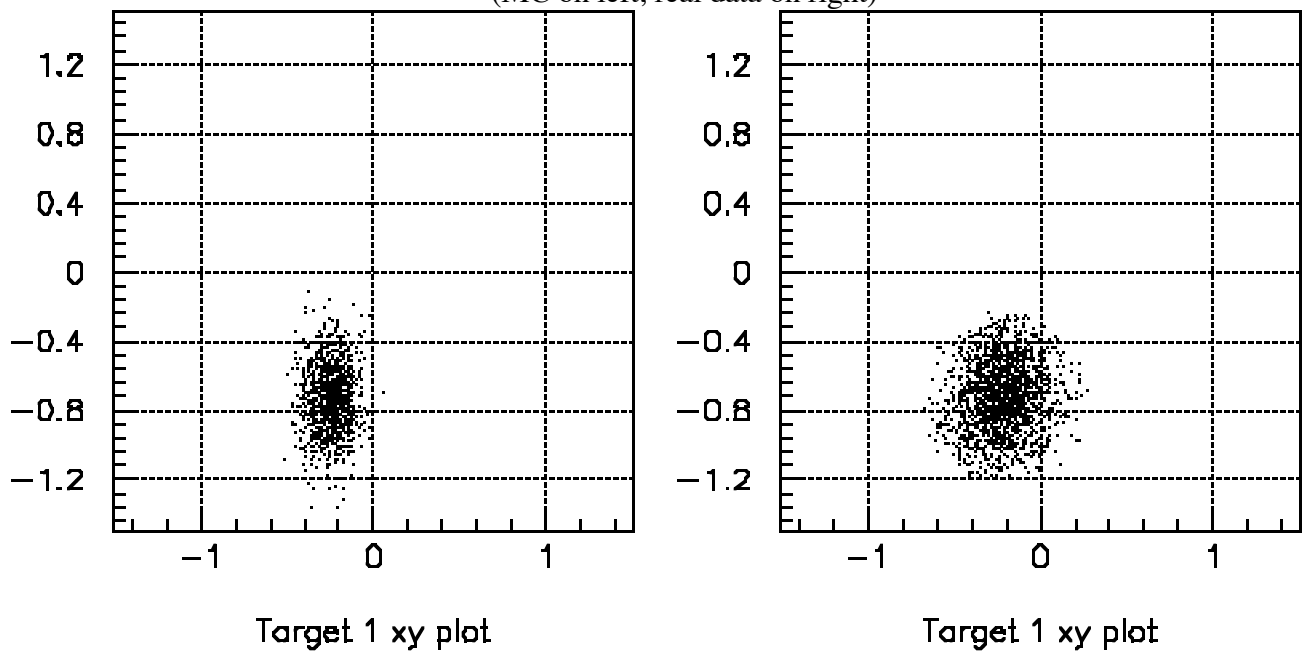


Figure 13
 X-Y Primary Vertex Positions in cm
 (MC on left; real data on right)



An area which might present a problem is the IERPM2 variable of each event. The

value of IERPM2 indicates the track multiplicity of the event. The SMD system is very efficient compared with the DC and usually generates many more tracks. Occasionally the SMDs detects a large (30+) number of tracks in an event. If the DST were to attempt to record all the tracks occurring in the SMD system, the event tape size would become very large and limit the number of events per tape. It would also increase the difficulty of track projection in the SESTR routine. An upper limit of 25 tracks has therefore been placed on the number of SMD tracks that are recorded on the DST tapes. The reconstruction program selects the 'best' 25 tracks on the basis of number of hits in different SMD planes and the error of that track. Any DC tracks are added in addition to the maximum number of SMD tracks. Plots of the IERPM2 values for both the MC and real data for each target are shown in Figure 14. The spike in the plot at ~ 25 shows the high number of events with large track multiplicities. A comparison of the real and MC data shows a substantial difference. The plots show two distinct structures, a 'bump' and a 'spike'. When the ratio of the height of the bump to the height of the spike is calculated for each target, a difference is observed. In the real data for Target 1 and 2, the ratios are approximately 1:8 and 1:4, respectively. For the MC data, the ratios are 1:11 and 1:11. This indicates that there are a higher percentage of large multiplicity events in Target 1 as compared to Target 2 in the real data than is present in the MC data. This could affect the target efficiency measurement.

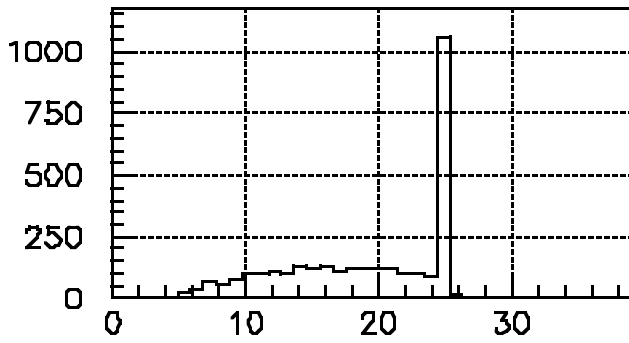
The real data shows that the percentage of large multiplicity events produced in the platinum target is higher than in the four carbon targets. This implies that the platinum event sample has more 'dirty' events, events with many tracks, which may or may not be tracks linked to $D^0 \rightarrow K\pi$ decays. This could make reconstruction of legitimate events more difficult and lower the efficiency in the platinum target. The MC generates roughly the same percentage of high IERPM2 events in each target, therefore there would be no drop in

efficiency for the platinum target. This would tend to raise the apparent efficiency of Target 1 events as calculated by the MC, hence lowering the actual number of events after the efficiency correction is applied.

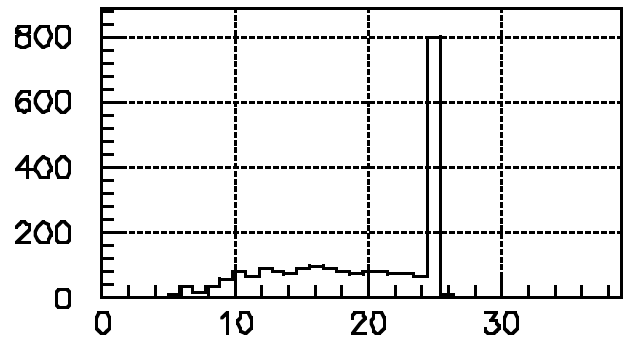
The remaining comparisons show that the MC and real data are similar. Two of the more important parameters are the Feynman X and PTB of the events. See Figure 15 for plots. The Feynman X variable, which is a measure of the fraction of beam energy carried by the D meson, and the PTB variable, the transverse momentum imbalance, measurements are within expectations. The PTB plot for the MC data is different from for the real data, but the MC data suffers no contamination from non-D meson tracks. Therefore, there would be few two track vertices where the transverse momentums did not balance according to the conservation of momentum. In the real data there would be many tracks that appeared to originate from the same vertex but would not represent a D meson decay, increasing high PTB hits. The Feynman X plot shows good agreement indicating that the DC hole is properly modeled within the MC.

A final check was performed. Using the truth table result for the number of events per target, a calculation of the A-dependence parameter, α , was performed. (See Chapter Two for details.) The value for α was part of the MC data files and was set to 0.75. The value calculated was 0.7502, very close to the set value.

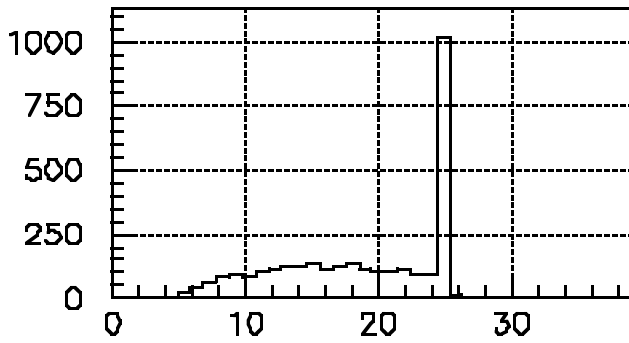
Figure 14
IEPRM2 Histograms
(MC on left; real data on right)



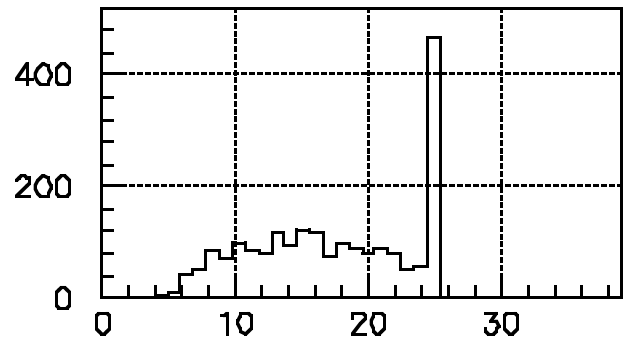
ierpm2 tgt 1



ierpm2 tgt 1

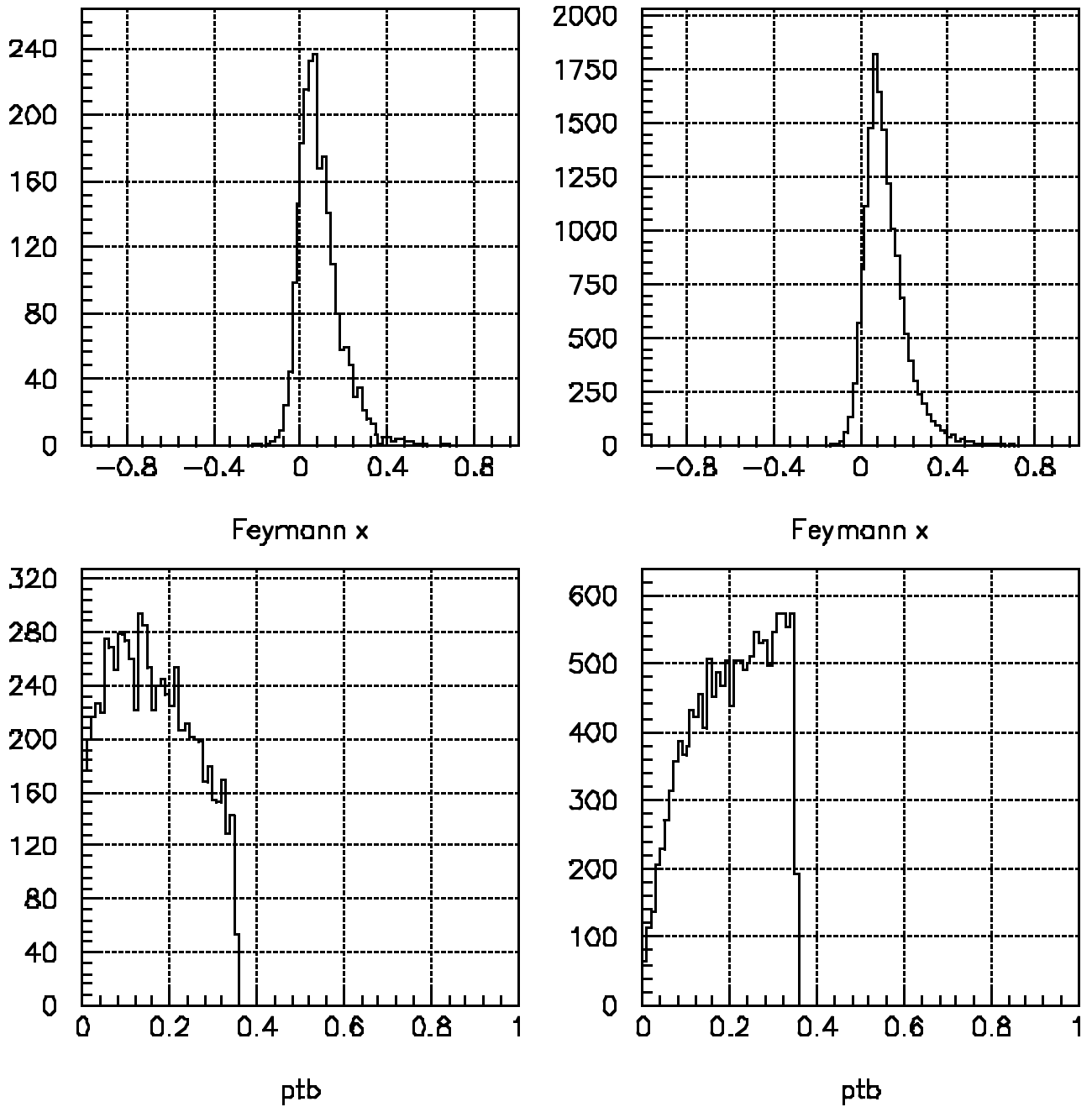


ierpm2 tgt 2



ierpm2 tgt 2

Figure 15
Feynman X and PTB Histograms
(MC on left;real data on right)



Chapter Eight: Results and Discussion

Using the number of events per target derived in the D meson stripping, the target efficiencies determined by the Monte Carlo simulation, the various target parameters, and the A-dependence formula (2.9) derived in Chapter Two, the value of α can be easily calculated. Two methods still remain, calculating α by comparing the platinum target to each carbon target separately or averaging the carbon targets. Both methods were used for both decay modes and the results appear in Tables 11 and 12.

Table 11
A-Dependence Values Calculated for Each Platinum-Carbon Target Pair.

Target Pairs	Value of α for D ⁰ Mode	Value of α for D ⁺ Mode
Target 1 - Target 2	$0.765^{+0.041}_{-0.046}$	$0.737^{+0.040}_{-0.046}$
Target 1 - Target 3	$0.758^{+0.039}_{-0.044}$	$0.735^{+0.041}_{-0.045}$
Target 1 - Target 4	$0.768^{+0.039}_{-0.044}$	$0.775^{+0.042}_{-0.046}$
Target 1 - Target 5	$0.762^{+0.039}_{-0.043}$	$0.767^{+0.043}_{-0.049}$

Table 12
A-Dependence Average Values

Average Value of α for D ⁰ Mode	Average Value of α for D ⁺ Mode
$0.763^{+0.040}_{-0.044}$	$0.754^{+0.036}_{-0.047}$

The error limits were calculated by adding the errors in quadrature. First the errors

in the events per target were added in quadrature. Then the errors in the efficiencies of the targets were added together. The errors on the target thickness and density were small enough ($> 1\%$) and could be disregarded. Both sets of errors were added in quadrature to find the total percent error in the corrected ratio of Equation (7.9). To take the natural logarithm of the corrected ratio (CR) and its error, α was calculated using the CR with no error. Then the error was added to the CR and the maximum value for α was found. The lower limit of α was found in the same manner.

The average value of α for each decay mode was determined by averaging the number of events occurring in the carbon targets and calculating its associated average error. These average numbers were then substituted in Equation (7.9) along with the values from the platinum target and α was measured and the errors evaluated.

The value of the A-dependence parameter has been measured in other experiments using a pion beam at several energies. Also, the interactions of a proton beam and nuclei have been used to measure α . Table 13 shows the various values along with beam type, energy, and x_F ranges.

Clearly, the values presented in Tables 11 and 12 are lower by $\sim 25\%$ and very close to the hard sphere scattering value of two-thirds. No clear explanation is forthcoming. Various experiments have examined the production of light hadrons at large transverse momenta (p_t) and have observed variations in α , usually increasing as p_t increases. [17], [18], [19] However, in E769, there appeared to be little variation in α as a function of transverse momentum for charm production. [20] In the same paper, the dependence of α on x_F was also shown to have been very small. This is not unexpected since the values of p_t and x_F which seem to show variations are much larger than the values seen in E791 and E769. Therefore the explanations for the low value of α must lie

elsewhere.

Table 13
Comparison of α Measurements

Experiment	Beam (GeV)	Beam Type	α	x_F Range
E769	250	Pion	1.00 ± 0.05	> 0.0
WA82	340	Pion	0.92 ± 0.06	> 0.0
WA78	320	Pion	0.81 ± 0.05	> 0.2
This Thesis	500	Pion	$\sim 0.76 \pm 0.04$	$-0.1 < x_F < 0.4$

A rough calculation shows that to measure a value of α near 1, there must be approximately twice as many events in the first, platinum target as in the carbon targets. Therefore, a search was carried out to learn if there was any reason for the lower than expected number of events in the platinum target (or conversely, if there was any reason for there to be more events in the carbon targets).

There are three possible areas in which errors might occur; the reconstruction, the Monte Carlo simulation, or the stripping routine and A-dependence calculation.

The reconstruction program is an extremely complex piece of FORTRAN code. A careful examination of the entire package would take a great deal of time and effort. The prime concern is the effectiveness of the VTXSTR vertexing subroutine. If VTXSTR should be inefficient at finding events in the platinum target, the measurement of α would be affected. The vertexing package has progressed through several versions and has been examined for errors. No major bugs have appeared in the recent code. Other areas in the program could be causing difficulties, but this is unlikely.

The stripping routine is very straightforward and was closely examined for any errors. Various changes were made in the cuts to determine if any bias was present that might alter the events observed in each target. Other areas were examined, including the particle track category that indicated the area where the tracks were observed. Tracks which were observed in multiple detectors and planes were given high category numbers while tracks which only occurred in one detector or few planes were given low numbers. It was thought that the platinum target might be producing more low category tracks which were not being projected into the DC system. This would result in fewer D mesons being reconstructed in the first target and, ultimately, lowering the A-dependence. Comparisons of the track categories present in the MC and real data showed some difference, but none significant enough to cause a change in the events per target.

Currently, there are two other groups examining A-dependence, one using a vertex-list driven strip the other using a candidate driven strip. No official results have been released, but it appears that the list driven strip is also generating an $\alpha \sim 0.75$, while the candidate driven strip gives an $\alpha \sim 0.88$. This suggests a possibility. In examining the Monte Carlo data, it was observed that a discrepancy existed in the IERPM2 values when compared to the real data. The real data had a higher percentage of platinum events with IERPM2 values (~ 25) compared to carbon events. The MC data does not model this variation, the percentage of high track multiplicity events is approximately equal in the first and second targets. The candidate driven search being carried out is examining all tracks for a track combination at a common vertex that has the desired mass. If the vertex list strip combines one track from a D meson with a false track, the real D meson cannot be formed, since tracks are not allowed to be in more than one secondary vertex. The chance of this occurring increases with track multiplicity. The candidate driven search that examines all

track pairs could catch such an event, even if the tracks did not form a secondary vertex in the reconstruction. Since the MC has a lower percentage of high IERPM2 events in the platinum, such loss of events would not be modeled, producing a higher apparent efficiency. There are physical reasons to expect higher track multiplicities for platinum events. The radiation length of platinum is about one-seventh that of carbon. The ability of a high energy photon to produce an electron-positron pair is dependent upon the radiation length of the material. The attenuation formula is;

$$I = I_0 e^{-\left(\frac{7x}{9X_0}\right)}, \quad (8.1)$$

where:

- I is the attenuation of the photon intensity due to pair production;
- I_0 is the incident photon intensity;
- x is the thickness of the material;
- X_0 is the radiation length of the material.

If values for the target thickness and radiation lengths are substituted into Equation (8.1), the ratio of carbon attenuation and platinum attenuation can be determined. According to this calculation the platinum target would create ten times as many electron-positron pairs than carbon targets for a given intensity of photons. These e^-/e^+ pairs produce tracks in the spectrometer. These tracks could be the tracks causing the higher values of IERPM2 observed. If the MC simulation is not correctly reproducing the production of e^-/e^+ pairs in the platinum, this could account for the observations.

Another reason to suspect the accuracy of the Monte Carlo comes from a study conducted prior to the latest release of the reconstruction and MC FORTRAN code. An

MC tape containing 10,000 $D^0 \rightarrow K + \pi$ events was written. This tape was reconstructed and processed, generating efficiencies for each target foil. However, these efficiencies are considerably different than those arising from the later MC tapes. An A-dependence calculation was made with these efficiencies producing an α of ~ 0.9 . The events from this early tape were examined in manner similar to the recent MC tapes, and found to be inconsistent with both the real data and newer MC events. The small sample size makes this comparison difficult however so the early MC data tape was not used. As yet no explanation for this alteration of the MC data has been found.

Finally, the unusual behavior of the D^+ MC events is worrisome. It could be caused by the slightly lower sample size, but the downward trend and the central dip in the efficiency appears to be significant in Figure 11. The data also appears to follow this trend which indicates that the MC is modeling the real events accurately, but the cause of the trend is not apparent. This trend was not apparent in the E769 analysis; both the D^+ and D^0 efficiencies followed the same general upward trend. [20]

Chapter Nine: Conclusions

Although the measured values of α appears to be low compared with other experiments which show an α of ~ 1 (indicating volume dependent cross sections) implementation of the Multi-stream Output stripper, the D meson strip, and the Monte Carlo simulation generated some insight into the process of charmed particle production. The comparison between the MC data and actual data showed subtle differences that might, with further study, explain the low result for α . Also, the different measurements from the vertex-list stripper and the candidate driven strippers indicate a possible inadequacy of the list driven approach. However, the theory behind the calculation of α appears to be sound, since it was able to reproduce the value encoded in the MC data file. The previous experimental results indicate room for improvement in the method of extracting the pertinent data from the DST tapes. I feel that further study should be devoted to the MC package and the stripping code, and perhaps another look at the vertexing program, VXTSTR.

Selected Bibliography

- [1] Particle Data Group, Review of Particle Properties, Physics Letters 239B, (1990) 1.
- [2] Colin W. Gay, The Charm Cross Section and Atomic Number Dependence in π -N Collisions, Ph.D. Thesis, University of Toronto (1991).
- [3] J. Ashman et al. (EM Collaboration), Physics Letters B202, (1988) 603.
- [4] R. Jedicke, Flavour Dependence of Hadroproduced Charm-Strange mesons, Ph.D Thesis, University of Toronto, 1991.
- [5] D.J. Summers et al., Charm Physics at Fermilab E791, Proceedings of the XXVIIth Recontre de Moriond, Electroweak Interactions and Unified Theories, Les Arcs, France (15-22 March 1992) 417.
- [6] General Electric Superabrasives, 6235 Huntly Road, Worthington, Ohio. 43805 USA.
- [7] P. Karchin et al. (E691), Test Beam Studies of a Silicon Microvertex Detector, IEEE Transactions in Nuclear Science 32, (1985) 612.
- [8] H. Fenker, E769 Internal Memo, C2 Gas Mixture Monitoring During E769, undated.
- [9] E. Aitala, E791 Internal Document, The LVMON System, 1991.
- [10] David Bartlett et al. (E691), Performance of the Cherenkov Counters in the Fermilab Tagged Photon spectrometer Facility, Nuclear Instruments and Methods A260, (1987) 55.
- [11] C.R. Kitchin, Astrophysical Techniques, Adam Hilger Ltd, Bristol, 1984.
- [12] D.J. Summers (E516), Reconstruction of a Strip Geometry Calorimeter Using Stepwise Regression, Nuclear Instruments and Methods 228, (1985) 290.
- [13] V. K. Bharadwaj et al. (E516), A Large Area Liquid Scintillation Multiphoton Detector, Nuclear Instruments and Methods 228, (1985) 283.
- [14] J. A. Appel, P. M. Mantach et al. (E516), Hadron Calorimetry at the Fermilab Tagged Photon Spectrometer Facility, Nuclear Instruments

and Methods A243, (1986) 361.

- [15] S. Amato, J.R.T. de Mello Neto, J. de Miranda, C. James, D.J. Summers, and S.B. Bracker, The E791 Parallel Architecture Data Acquisition System, Nuclear Instruments and Methods A324, (1993) 535.
- [16] C. Stoughton and D. J Summers (E769), Using Multiple RISC CPUs in Parallel to Study Charm Quarks, Computers in Physics 6, (1992) 371.
- [17] M. Adamovich et al. (WA82), Nuclear Dependence of Charm Production by a 340 GeV π^- Beam, Physics Letters B284 (1992) 453.
- [18] H. Cobbaert et al. (WA78), A-Dependence of the Charm Production Cross Section in 320 GeV/c π^- Interactions, Physics Letters B191, (1987) 456.
- [19] J.W. Cronin et al., Production of Hadrons with Large Transverse Momentum at 200 GeV and 300 GeV, Physical Review Letters 31 (1973) 1426.
- [20] G.A. Alves et al. (E769), Atomic Mass Dependence of D^\pm and D^0 , \underline{D}^0 Production in 250 GeV π^\pm - Nucleon Interactions, Physical Review Letters 70 (1993) 722.

Other useful references of experiments and particle physics in general:

- G.A. Alves et al. (E769), $D^{*\pm}$ Production in 250 GeV π^\pm - Nucleon Interactions, FERMILAB-PUB-93-081-E (April 1993); (Submitted to Physical Review Letters).
- D. Antreasyan et al., Production of Hadrons at Large Transverse Momentum in 200 GeV, 300 GeV and 400 GeV pp and pN Collisions, Physics Review D19, (1979) 764.
- V. K. Bharadwaj et al. (E516), An Inexpensive Large Area Shower Detector with High Spatial and Energy Resolution, Nuclear Instruments and Methods 155, (1978) 411.
- L.M. Cremaldi et al., Fermilab E791, Proceedings of the XXVI International Conference on High Energy Physics, Dallas, Texas (6-12 August 1992) 1058.
- D. Griffiths, Introduction to Elementary Particle Physics, J. Wiley & Sons, 1987.

L. Kluberg, et al., Atomic Number Dependence of Large Transverse Momentum Hadron Production by Protons, *Physical Review Letters* 38, (1977) 670.

D. Perkins, Introduction to High Energy Physics, Addison-Wesley, 1987.

Ronald A. Sidwell, E791 Status Report, Proceedings of the Fermilab Meeting of DPF 92, Batavia, Illinois (10-24 November 1992) 672.

Appendix A. A Sample Stripping Subroutine

This is a sample of one of the D meson strip subroutines. All four subroutines followed the same general format, the only major differences were in the histograms produced, cuts applied, or parameters that were examined in closer detail. The subroutine presented was the most complex of the four; it was used to examine the D^0 meson data very closely for variations in IERPM2 values and track categories. All major variables have been commented with the exception of global variables used in all the E791 code.

```
*****
```

```
*****
```

```
subroutine kpi_st_tgt (istrip)
```

```
implicit none
```

```
save
```

```
C-- True if event is accepted by this strip, otherwise false
```

```
logical*4 istrip
```

```
C-- Information about tracks, vertices... in the current event
```

```
Include '/usr/tools/f791/includes/switch.inc'
```

```
Include '/usr/tools/f791/includes/param_trk.inc'
```

```
Include '/usr/tools/f791/includes/param_ttt.inc'
```

```
Include '/usr/tools/f791/includes/param_ntk.inc'
```

```
Include '/usr/tools/f791/includes/param_beam.inc'
```

```
Include '/usr/tools/f791/includes/param_vtx.inc'
```

```

Include '/usr/tools/f791/includes/tracks.inc'
Include '/usr/tools/f791/includes/beamout.inc'
Include '/usr/tools/f791/includes/vtxpar.inc'
Include '/usr/tools/f791/includes/vxxkep.inc'
Include '/usr/tools/f791/includes/tkpars.inc'
Include '/usr/tools/f791/includes/savevt.inc'
Include '/usr/tools/f791/includes/ckvid.inc'
Include '/usr/tools/f791/includes/calsum.inc'
Include '/usr/tools/f791/includes/caldst.inc'
Include '/usr/tools/f791/includes/pizout.inc'
Include '/usr/tools/f791/includes/esum791.inc'
external effm2,effm3,xf

```

```

C--    invariant mass routines
      real effm2,effm3

C--    secondary vertex number (2, 3...)
      integer*4  ivert

C--    Track indices for the two tracks in a 2-prong vertex
      integer*4  it1, it2

C--    invariant mass of the pion/kaon D0 candidate
      real*4  kpi_mass

C--    Transverse momentum balance of the vertex
      real*4  ptb, real_ptb

```

C-- Unused parameters returned from ptbvtx
 real*4 p1, p2, p3, p, cx, cy, cz

C-- param for xf calc
 real*4 pxd,pyd,pzd,e_d, xf_val,xf

C-- Z position of the secondary vertex
 real*4 z_vtx, vx, vy

C-- Z separation, primary and secondary vertex
 real*4 vdz

C-- Error in Z separation, primary and secondary vertex
 real*4 vez

C-- SdZ (vertex separation / error in separation)
 real*4 sdz

C-- decay assymetry $(p2-p1)/(.5*(p2+p1))$
 real*4 pra

C-- proper lifetime in ps calculated from decay length- $dz=\beta*\gamma*c*\tau$
 real*4 tau

C-- target variables for tgif calculation
 real*4 tgif(50),tgtd,tgtz(6),tgti
 integer*4 itgt(50)

C-- target z positions

data tgtz/-8.123,-6.646,-5.110,-3.575,-2.036,-0.087/

- C-- dummy variables
integer i,k,qq
- C-- Pt balance cut (gev)
real*4 ptb_max
parameter (ptb_max = 0.35)
- C-- decay assymetry $pra = (p2-p1)/(p2+p1)$
real*4 pra_max
parameter (pra_max = 0.75)
- C-- SdZ cut (cm / cm)
real*4 sdz_min
parameter (sdz_min = 8.0)
- C-- proper lifetime in ps calculated from decay length- $dz = \beta * \gamma * c * \tau$
real*4 tau_max
parameter (tau_max = 2.0)
- C-- D0 mass window (gev)
real*4 kpi_min, kpi_max
parameter (kpi_min = 1.7)
parameter (kpi_max = 2.1)
- C-- pion and kaon rest masses
real*4 pi_mass, k_mass

```

parameter (pi_mass =      0.139568)
parameter (k_mass  =      0.493646)

```

C-- minimum and maximum secondary vertex Z

```

real*4 zmin, zmax
parameter (zmin = -10.00)
parameter (zmax = +28.000)

```

C-- jcat parameters

```

real*4 jcat1,jcat2, jcatq,ierpm2_ctr,ierpm2_real real*4
ier_1_gd,ier_2_gd,ier_3_gd,ier_4_gd,ier_5_gd

logical*4 first_time /.true./

ier_1_gd = 0.
ier_2_gd = 0.
ier_3_gd = 0.
ier_4_gd = 0.
ier_5_gd = 0.

```

C-- First time through, book the histograms

```

if (first_time) then
  first_time = .false.
  call hbook1(14099,'kpi mso stripper',80, 1.7,2.1,0.)
  call hbook1(4999,'Primary vertex position',1000,-9.0,1.0,0.)

  call hbook1(14999,'Target 1 prim. vtx',1000,-9.0,1.0,0.)

```


call hbook1(24999,'Target 2 prim. vtx',1000,-9.0,1.0,0.)

call hbook1(34999,'Target 3 prim. vtx',1000,-9.0,1.0,0.)

call hbook1(44999,'Target 4 prim. vtx',1000,-9.0,1.0,0.)

call hbook1(54999,'Target 5 prim. vtx',1000,-9.0,1.0,0.)

call hbook1(5000,'Secondary vertex position',100,-9.0,1.0,0.)

call hbook1(4086,'Mass os all K-pi pairs',80,1.7,2.1,0.)

call hbook1(5001,'Feymann x',100, -1.0, 1.0, 0.)

call hbook1(10,'ptb',101, 0.0, 1.0, 0.)

call hbook2(88888, 'xf vs ierpm2', 100, -1.0,

+ 1.0, 30, 0.0, 29.0, 0.)

call hbook2(19086,'Target 1 xy plot',50, -1.5,

+ 1.5, 50, -1.5,1.5, 0.)

call hbook2(29086,'Target 2 xy plot',50, -1.5,

+ 1.5, 50, -1.5,1.5, 0.)

call hbook2(39086,'Target 3 xy plot',50, -1.5,

+ 1.5, 50, -1.5,1.5, 0.)

call hbook2(49086,'Target 4 xy plot',50, -1.5,

+ 1.5, 50, -1.5,1.5, 0.)

call hbook2(59086,'Target 5 xy plot',50, -1.5,

+ 1.5, 50, -1.5,1.5, 0.)

call hbook1(14086,'Target 1 K-pi mass',80,1.7,2.1,0.)

call hbook1(24086,'Target 2 K-pi mass',80,1.7,2.1,0.)

call hbook1(34086,'Target 3 K-pi mass',80,1.7,2.1,0.)
call hbook1(44086,'Target 4 K-pi mass',80,1.7,2.1,0.)
call hbook1(54086,'Target 5 K-pi mass',80,1.7,2.1,0.)

call hbook1(17086,'k-pi mass Pt (0,10)',80, 1.7,2.1,0.)
call hbook1(27086,'k-pi mass C (0,10)',80,1.7,2.1,0.)
call hbook1(37086,'k-pi mass all (0,10)',80, 1.7,2.1,0.)
call hbook1(47086,'k-pi mass Pt (10,20)',80, 1.7,2.1,0.)
call hbook1(57086,'k-pi mass C (10,20)',80, 1.7,2.1,0.)
call hbook1(67086,'k-pi mass all (10,20)',80, 1.7,2.1,0.)
call hbook1(77086,'k-pi mass Pt (20+)',80,1.7,2.1,0.)
call hbook1(87086,'k-pi mass C (20+)',80, 1.7,2.1,0.)

call hbook1(97086,'k-pi mass all (20+)',80, 1.7,2.1,0.)

call hbook1(186,'tgt1 jcat all',20,0,19,0.)
call hbook1(286,'tgt2 jcat all',20,0,19,0.)

call hbook1(386,'tgt3 jcat all',20,0,19,0.)

call hbook1(486,'tgt4 jcat all',20,0,19,0.)

call hbook1(586,'tgt5 jcat all',20,0,19,0.)

call hbook1(661,'tgt1 jcat ierpm2 gt 24',20,0,19,0.)
call hbook1(662,'tgt2 jcat ierpm2 gt 24',20,0,19,0.)
call hbook1(663,'tgt3 jcat ierpm2 gt 24',20,0,19,0.)

```

call hbook1(664,'tgt4 jcat ierpm2 gt 24',20,0,19,0.)

call hbook1(665,'tgt5 jcat ierpm2 gt 24',20,0,19,0.)

call hbook1(881,'tgt1 ierpm2 if jcat gt 3',40,0,39,0.)

call hbook1(882,'tgt2 ierpm2 if jcat gt 3',40,0,39,0.)

call hbook1(883,'tgt3 ierpm2 if jcat gt 3',40,0,39,0.)

call hbook1(884,'tgt4 ierpm2 if jcat gt 3',40,0,39,0.)

call hbook1(885,'tgt5 ierpm2 if jcat gt 3',40,0,39,0.)

call hbook1(1111, 'ierpm2', 40,0,39,0.)

call hbook1(771, 'ierpm2 tgt 1', 40,0,39,0.)
call hbook1(772, 'ierpm2 tgt 2', 40,0,39,0.)
call hbook1(773, 'ierpm2 tgt 3', 40,0,39,0.)
call hbook1(774, 'ierpm2 tgt 4', 40,0,39,0.)
call hbook1(775, 'ierpm2 tgt 5', 40,0,39,0.)

end if

```

```

C--      find primary vtx z position

          tgti = 100

          tgtd = 0

          do k=1,6

          tgtd=xyzvtx(3,1) - tgtz(k)

```

```

if (abs(tgti) .gt. abs(tgtd)) then
  tgti=tgtd
  tgtf(1)=abs(tgti)
  itgt(1)=k
endif
end do

```

C-- find tgt xy distribution and all track numbers

```

call hf1 (4999, xyzvtx(3,1), 1.) vx=xyzvtx(1,1)
vy=xyzvtx(2,1)
ierpm2_ctr=ierpm2
  if (itgt(1) .eq. 1) then
    call hf2(19086,vx,vy,1.)
    call hf1(771,ierpm2_ctr,1)
    do qq = 1,ierpm2
      jcatq=jcatsg(qq)
      if (jcatsg(qq) .ge.3) then
        ier_1_gd=ier_1_gd+1.
      end if
      if (ierpm2.gt.24) then
        call hf1(661,jcatq,1.)
      endif
      call hf1(186,jcatq,1.)
    end do
  end if
end do

```

```
call hf1(881,ier_1_gd,1.)
endif
if (itgt(1) .eq. 2) then
call hf2(29086,vx,vy,1.)
call hf1(772,ierpm2_ctr,1.)
do qq = 1,ierpm2
if (jcatsg(qq) .ge.3) then
ier_2_gd= ier_2_gd+1.
end if
jcatq=jcatsg(qq)
if (ierpm2.gt.24) then
call hf1(662,jcatq,1.)
endif
call hf1(286,jcatq,1.)
end do
call hf1(882,ier_2_gd,1.)
endif
if (itgt(1) .eq. 3) then
call hf2(39086,vx,vy,1.)
call hf1(773,ierpm2_ctr,1.)
do qq = 1,ierpm2
if (jcatsg(qq) .ge.3) then
ier_3_gd= ier_3_gd+1.
end if
```

```
        jcatq=jcatsg(qq)
        if (ierpm2.gt.24) then
            call hf1(663,jcatq,1.)
        endif
        call hf1(386,jcatq,1.)
    end do
    call hf1(883,ier_3_gd,1.)
endif

if (itgt(1) .eq. 4) then
    call hf2(49086,vx,vy,1.)
    call hf1(774,ierpm2_ctr,1.)
    do qq = 1,ierpm2
        if (jcatsg(qq) .ge.3) then
            ier_4_gd= ier_4_gd+1.
        end if
        jcatq=jcatsg(qq)
        if (ierpm2.gt.24) then
            call hf1(664,jcatq,1.)
        endif
        call hf1(486,jcatq,1.)
    end do
    call hf1(884,ier_4_gd,1.)
endif

if (itgt(1) .eq. 5) then
```

```

call hf2(59086,vx,vy,1.)
call hf1(775,ierpm2_ctr,1.)
do qq = 1,ierpm2
  if (jcatsg(qq) .ge.3) then
    ier_5_gd= ier_5_gd+1.
  end if
  jcatq=jcatsg(qq)
  if (ierpm2.gt.24) then
    call hf1(665,jcatq,1.)
  endif
  call hf1(586,jcatq,1.)
end do
call hf1(885,ier_5_gd,1.)

```

```
endif
```

```

C-- fill ierpm3 histo
ierpm2_real=ierpm2
call hf1(1111,ierpm2_real, 1.)

```

```

C-- For every secondary vertex . . .
do ivert = 2, nvert

  jcat1=jcatsg(it1)
  jcat2=jcatsg(it2)

```

```

C--      If this vertex has exactly two associated tracks . . .
        if (ntkvtx (ivert) .eq. 2) then

C--      Fetch the two track indices
        it1 = itkvtx (1, ivert)
        it2 = itkvtx (2, ivert)

C--      If both tracks are category 3-15 . . .
        if (jcatsg(it1) .ge. 3 .and. jcatsg(it1) .le. 15 .and.
+         jcatsg(it2) .ge. 3 .and. jcatsg(it2) .le. 15) then

C--      If the total charge at the vertex is zero . . .
        if (q(it1) .eq. -q(it2)) then

C--      If the Z position of the vertex is reasonable . . .
        z_vtx = xyzvtx (3, ivert)
        if (z_vtx .ge. zmin .and. z_vtx .le. zmax) then

C--      Compute the transverse momentum balance, and cut on it
        call ptbvtx (ivert, p1, p2, p3, p, cx, cy, cz, ptb)
        if (ptb .lt. ptb_max) then
            real_ptb=ptb
            call hf1(10, real_ptb,1.)

C--      Compute the decay assymetry and cut on it
        call prat (it1, it2, pra)
        if (pra .lt. pra_max) then

```



```

C--          Compute SdZ and cut on it
vdz = z_vtx - xyzvtx(3,1)
vez = sqrt (errvtx (3, 1)**2 + errvtx (3, ivert)**2)
vez = max (vez, 0.0001)
sdz = vdz / vez
if (sdz.gt. sdz_min) then

C--          Compute the proper lifetime and cut on it
tau = 62.31 * vdz / (pp(it1) + pp(it2))
if (tau.lt. tau_max) then

C--          Compute the invariant mass (kaon, pion)
call m2bod (it1, it2, k_mass, pi_mass, kpi_mass)

c          kpi_mass = effm2(it1,it2,4,3)

C--          Compute tgtf value...

          tgti = 100
          tgtd = 0

          do k=1,6
          tgtd=xyzvtx(3,ivert) - tgz(k)
          if (abs(tgti) .gt. abs(tgtd)) then
              tgti=tgtd
              tgtf(ivert)=abs(tgti)
              itgt(ivert)=k

```

```
endif
end do
```

C--

If it lies in the D0 mass window, accept the event

```
if (kpi_mass .gt. kpi_min .and.
```

```
+      kpi_mass .lt. kpi_max) then
```

```
    if (tgtf(ivert) .gt. 0) then
```

```
      if (cprb2(it1,4) .gt. 0.16) then
```

```
        istrip = .true.
```

```
        if (ierpm2 .ge. 0 .and. ierpm2 .le. 10) then
```

```
          if (itgt(1) .eq. 1) then
```

```
            call hf1(17086,kpi_mass,1.)
```

```
          else
```

```
            call hf1(27086,kpi_mass,1.)
```

```
          endif
```

```
          call hf1(37086,kpi_mass,1.)
```

```
        endif
```

```
        if (ierpm2 .gt. 10 .and. ierpm2 .le. 20) then
```

```
          if (itgt(1) .eq. 1) then
```

```
            call hf1(47086,kpi_mass,1.)
```

```
          else
```

```
            call hf1(57086,kpi_mass,1.)
```

```
          endif
```

```
        call hf1(67086,kpi_mass,1.)
endif

if (ierpm2 .gt. 20) then
    if (itgt(1) .eq. 1) then
        call hf1(77086,kpi_mass,1.)
    else
        call hf1(87086,kpi_mass,1.)
    endif
    call hf1(97086,kpi_mass,1.)
endif

call D_MOM(it1,it2,kpi_mass,pxd,pyd,pzd,e_d)
xf_val=xf(pzd,e_d)
call hf1 (5001, xf_val, 1.)
call hf2 (88888, xf_val, ierpm2_real, 1.)

call hf1 (4086, kpi_mass, 1.)

call hf1 (5000, xyzvtx(3,ivert), 1.)

    if (itgt(1) .eq. 1) then
        call hf1(14086,kpi_mass,1.)
        call hf1(14999, xyzvtx(3,1), 1.)
    endif

    if (itgt(1) .eq. 2) then
```

```

call hf1(24086,kpi_mass,1.)
call hf1(24999, xyzvtx(3,1), 1.)
endif
if (itgt(1) .eq. 3) then
call hf1(34086,kpi_mass,1.)
call hf1(34999, xyzvtx(3,1), 1.)
endif
if (itgt(1) .eq. 4) then
call hf1(44086,kpi_mass,1.)
call hf1(44999, xyzvtx(3,1), 1.)
endif
if (itgt(1) .eq. 5) then
call hf1(54086,kpi_mass,1.)
call hf1(54999, xyzvtx(3,1), 1.)
endif
endif
endif
end if

C--      Compute the invariant mass (pion, kaon)
call m2bod (it1, it2, pi_mass, k_mass, kpi_mass)
c      kpi_mass = effm2(it1,it2,3,4)

C--      If it lies in the D0 mass window, accept the event

```

```

if (kpi_mass .gt. kpi_min .and.
+   kpi_mass .lt. kpi_max) then

    if (tgtf(ivert).gt. 0) then
        if (cprb2(it2,4) .gt. 0.16) then

            istrip = .true.

            if (ierpm2 .ge. 0 .and. ierpm2 .le. 10) then
                if (itgt(1) .eq. 1) then
                    call hf1(17086,kpi_mass,1.)
                else
                    call hf1(27086,kpi_mass,1.)
                endif
                call hf1(37086,kpi_mass,1.)
            endif

            if (ierpm2 .gt. 10 .and. ierpm2 .le. 20) then
                if (itgt(1).eq. 1) then
                    call hf1(47086,kpi_mass,1.)
                else
                    call hf1(57086,kpi_mass,1.)
                endif
                call hf1(67086,kpi_mass,1.)
            endif

            if (ierpm2 .gt. 20) then

```

```
if (itgt(1) .eq. 1) then
    call hf1(77086,kpi_mass,1.)
else
    call hf1(87086,kpi_mass,1.)
endif

call hf1(97086,kpi_mass,1.)
endif

call D_MOM(it1,it2,kpi_mass,pxd,pyd,pzd,e_d)
xf_val=xf(pzd,e_d)
call hf1 (5001, xf_val, 1.)
call hf2 (88888, xf_val, ierpm2_real,1.)
call hf1 (4086, kpi_mass, 1.)
call hf1 (5000, xyzvtx(3,ivert), 1.)

if (itgt(1) .eq. 1) then
    call hf1(14086,kpi_mass,1.)
    call hf1(14999,xyzvtx(3,1), 1.)
endif

if (itgt(1) .eq. 2) then
    call hf1(24086,kpi_mass,1.)
    call hf1(24999, xyzvtx(3,1), 1.)
endif

if (itgt(1) .eq. 3) then
    call hf1(34086,kpi_mass,1.)
```

```

call hf1(34999, xyzvtx(3,1), 1.)
endif
if (itgt(1) .eq. 4) then
call hf1(44086,kpi_mass,1.)
call hf1(44999, xyzvtx(3,1), 1.)
endif
if (itgt(1) .eq. 5) then
call hf1(54086,kpi_mass,1.)
call hf1(54999, xyzvtx(3,1), 1.)
endif
endif
endif
endif
return
end if
end if
end if
end if
end if
end if
end if
end if
end do
```

```
C--      This event is not accepted
        istrict = .false.
        return

        end
```


Biographical Sketch of the Author

The author, Eric Matthew Aitala, was born April 30, 1966 to Mr. and Mrs Franco Aitala, in upstate New York. Franco Aitala immigrated to the United States from Italy in 1960. Marilyn Aitala (nee Bemis) was born in Hamilton, NY.

He attended High School at Springfield HS in Springfield, Pennsylvania from 1980 to 1984 and graduated in 1984. He then attended The Pennsylvania State Univeristy from 1984 to 1988, where he received a Bachelor of Science degree in Astronomy in May, 1988. Eric then studied at The University of Mississippi, in the field of Physics, from 1989 to 1993 with the UM High Energy Physics Group. During the course of his enrollment, he worked on the E791 HEP Collaboration at Fermilab in Batavia, Illinois from 1989 to 1993.

Eric also taught and helped to develop the undergraduate Astronomy Laboratory and Astronomy Open House at Ole Miss and is one of the Astronomy Lab Manual's authors along with Dr. Donald Summers. Eric also presented various talks to local school children on the subject of Astronomy. His interests include Ultimate Frisbee and foil fencing, having helped to establish the Fencing Clubs at Penn State and Ole Miss.

Mr. Aitala plans on returning to the field of Astronomy and will be attending The Michigan State University starting in the Fall of 1993. He plans on working in the field of high energy Astrophysics and Cosmology. Ultimately, he plans on receiving a Ph.D. and working both in research and education.

His permanent address is:

Eric Aitala
517 Lawrence Drive
Springfield, PA 19064

